

1 **High-resolution hybrid MODIS-Landsat estimation of post-monsoon**
2 **agricultural burned area in northwestern India**

3 Tianjia Liu^{a,b}, Miriam E. Marlier^c, Alexandra N. Karambelas^d, Meha Jain^e, Sukhwinder
4 Singh^e, Manoj K. Singh^f, Ritesh Gautam^g and Ruth S. DeFries^c

5 *^aDepartment of Earth and Environmental Sciences, Columbia University, New York,*
6 *USA*

7 *^bDepartment of Earth and Planetary Sciences, Harvard University, Cambridge, USA*

8 *^cDepartment of Ecology, Evolution, and Environmental Biology, Columbia University,*
9 *New York, USA*

10 *^dThe Earth Institute, Columbia University, New York, USA*

11 *^eSchool for Environment and Sustainability, University of Michigan, Ann Arbor, USA*

12 *^fDepartment of Mathematics, University of Petroleum and Energy Studies, Dehradun,*
13 *Uttarakhand, India*

14 *^gEnvironmental Defense Fund, Washington DC, USA*

15 Corresponding author: Tianjia Liu (tianjialiu@g.harvard.edu)

16 High-resolution hybrid Landsat-MODIS estimation of post-monsoon agricultural
17 burned area in northwestern India

18 A leading source of outdoor emissions in northwestern India comes from crop
19 residue burning after the annual monsoon (*kharif*) and winter (*rabi*) crop
20 harvests. Agricultural burned area, from which agricultural fire emissions are
21 derived, is difficult to quantify due to the mismatch between moderate-resolution
22 satellite sensors and the relatively small size and short burn duration of the fires.
23 Many previous atmospheric science studies use the Global Fire Emissions
24 Database (GFED), which is based on the Moderate Resolution Imaging
25 Spectroradiometer (MODIS) burned area product MCD64A1, as a bottom-up
26 outdoor fires emissions dataset. Correction factors with MODIS active fire
27 detections have previously attempted to account for small fires. Here, we present
28 a burned area classification algorithm that leverages more frequent MODIS
29 surface reflectance (SR) observations (daily, 500 m) with higher spatial
30 resolution Landsat (every 16 days, 30 m) SR observations to boost and refine
31 MCD64A1 burned area at 30-m spatial resolution. Our hybrid MODIS and
32 Landsat approach is based on two-tailed, quantile-based Normalised Burn Ratio
33 (NBR) thresholds, abbreviated as ModL2T, and results in an estimated $66 \pm 31\%$
34 higher burned area than MCD64A1 in northwestern India during the 2003-2016
35 post-monsoon (October to November) burning seasons. Previous underestimation
36 of agricultural burned area suggests that the public health impacts estimates from
37 post-monsoon fires in this region are also conservative. We find moderate
38 agreement between village-level fraction of ModL2T-derived burned area and
39 surveyed farmers who burned crop residue, normalised by landholding area ($r =$
40 $0.62, p < 0.01$), in 2016. However, sources of error still arise from small median
41 landholding sizes (1-3 ha), heterogeneous spatial distribution of two dominant
42 burning practices (partial and whole field), moderate to coarse spatio-temporal
43 satellite resolution, dark soil background, cloud and haze contamination, and
44 possible conflation of burning with harvest. Our results suggest that fusion
45 methods using moderate and high resolution satellite imagery can improve
46 agricultural fire emissions inventories, thus allowing for more accurate
47 assessments of the contribution of post-monsoon agricultural fires to air quality
48 degradation and related population-weighted smoke pollution exposure in
49 northwestern India.

50 Keywords: fires; crop residue; burned area; MODIS; Landsat

51 **1. Introduction**

52 ***1.1. Agricultural residue burning in northwestern India***

53 India is embracing agricultural mechanisation to increase crop productivity and
54 decrease labour costs in order to feed its rapidly growing population (Mehta et al.
55 2014). Agriculture in India is currently 40-45% mechanised, below that of the United
56 States, Russia, Western Europe, China and Brazil (57-95%) (Bai 2014; Mehta et al.
57 2014). India's population is expected to grow from 1.3 billion in 2015 to 1.7 billion by
58 2050 (UN 2015). This population surge demands sustainable increases in crop
59 productivity, intensity and yield, which in turn affects the rise of agricultural
60 mechanisation. Traditionally, farmers collect crop residue to feed livestock. However,
61 as India mechanises, farmers are using combine harvesters, which leave behind
62 scattered crop residues that are labour intensive to remove manually (Vadrevu et al.
63 2011; Kumar et al. 2015). Consequently, 80-90% of crop residue left behind by
64 combine harvesters is burned in field, which can severely degrade regional air quality
65 seasonally (Sidhu and Beri 2005; Government of India 2007; Singh et al. 2008; Gupta
66 2012; Liu et al. 2018). More accurate burned area estimation is a critical prerequisite for
67 improving 'bottom-up' fire emissions inventories and quantifying public health impacts
68 from air quality degradation. In this study, we target these episodic agricultural fires and
69 build on existing methods for moderate-resolution burned area classification by
70 integrating with complementary high-resolution satellite imagery for this region.

71 In northwestern India, the timing of the double cropping system particularly
72 limits the timeframe to clear the fields of monsoon crop residue (primarily rice) during
73 the post-monsoon (October to November). Because farmers must market rice at the
74 earliest time possible and have limited time to sow the winter crop (primarily wheat),
75 they often burn the crop residue (Jain et al. 2014; PRSC 2015; Ahmed et al. 2015;
76 Gupta 2012). Thus, in spite of the restrictions on agricultural burning, farmers continue
77 to burn crop residue due to the lack of viable, well-incentivised and cost-effective
78 alternatives (Kumar et al. 2015; Ahmed et al. 2015; Gupta 2012).

79 Smoke plumes from crop residue burning blankets rural and urban areas within
80 the Indo-Gangetic Plains (IGP), which includes Punjab and Haryana, during the post-
81 monsoon (October to November) burning season (Figure 1). During pre-monsoon (April
82 to May), wheat residue is burned to prepare fields for sowing the monsoon crop. In
83 general, carbonaceous particles can be transported hundreds of kilometres in the
84 atmosphere (Sharma et al. 2010; Kaskaoutis et al. 2014). Besides air quality degradation
85 and public health impacts, crop residue burning reduces soil quality by depleting
86 organic matter, major nutrients, and microbial biomass (PRSC 2015). This inhibits the
87 productivity of the next cropping season. However, previous work using satellite fire
88 detections and HYSPLIT atmospheric back trajectories suggests that pre-monsoon
89 wheat residue burning is of less concern to the Delhi National Capital Region's air
90 quality than post-monsoon rice residue burning due to different atmospheric transport
91 patterns, higher ventilation from high boundary layer conditions, and less overall fire
92 intensity (Liu et al. 2018). While Delhi's average post-monsoon 'airshed,' or the
93 approximate region that can contribute to Delhi's air quality, encompasses most of
94 Haryana and Punjab, the average pre-monsoon Delhi airshed shifts southward, avoiding
95 high fire intensity areas. In addition, the influence of desert dust emissions and transport
96 in the post-monsoon season is minimal, in comparison to the strong dust activity during
97 pre-monsoon months (April to June), originating from the Thar desert as well as long-

98 range transport from the Arabian Peninsula. Therefore, the burned area mapping and its
99 quantification in this study is focused on the post-monsoon season.

100 [FIGURE 1]

101 *1.2. Burned area estimation of small fires*

102 The MODIS burned area product MCD64A1 (Giglio et al. 2009), on which the Global
103 Fire Emissions Database, version 4 (GFEDv4) emissions are based (Giglio et al. 2013),
104 underestimates the contribution of small fires, which has been generally accounted for
105 with a scale factor (van der Werf et al. 2010; 2017; Randerson et al. 2012; Zhu et al.
106 2017). MCD64A1 is limited by its moderate spatial resolution of 500 m x 500 m. In
107 particular, small fires < 120 ha are not well-detected (Zhu et al. 2017). Many active fires
108 in croplands are found outside the estimated burned area extent, because the
109 conservative detection threshold for burned area estimation often misses small fires
110 (Randerson et al. 2012; Zhu et al. 2017). GFEDv4s, which includes a small fires boost
111 to GFEDv4, added 79-123% in burned area to the cropland-related classes, but
112 Randerson et al. (2012) suggest that the estimate is still conservative. Thus, higher
113 spatial resolution satellite imagery is a necessary prerequisite to more accurately
114 estimate burned area from small agricultural fires.

115 The differenced Normalised Burn Ratio (dNBR) characterises the burn extent
116 and severity of most fires over 2 km² in area on public lands (Key and Benson 2006).
117 dNBR is the difference in pre-fire and post-fire NBR. NBR is defined as:

$$118 \quad \text{NBR} = \frac{\rho_{NIR} - \rho_{SWIR}}{\rho_{NIR} + \rho_{SWIR}} \quad (1)$$

119 in which ρ_{NIR} and ρ_{SWIR} represent the surface reflectance at near infrared and
120 shortwave infrared wavelengths, respectively. Additionally, Picotte and Robertson
121 (2010) find that dNBR is suitable to map many small fires within a large landscape; this
122 is particularly relevant for agricultural fires, which are small in size and tends to cluster
123 spatially. Indeed, global and region-specific studies have used NBR-based approaches
124 to estimate small fires, including agricultural fires (e.g. Oliva and Schroeder 2015;
125 McCarty et al. 2008, 2009; Randerson et al. 2012; Zhu et al. 2017; Hall et al. 2016;
126 Wang et al. 2018). NBR is an effective indicator in mapping burn scars due to the
127 accuracy of classification with the SWIR bands (Avery and Berlin 1992; Eva and
128 Lambin 1998; Veraverbeke et al. 2010) and avoidance of smoke and dust susceptibility,
129 unlike bands in the visible range of the spectrum (White et al. 1996; Roy 1999; Rogan
130 and Yool 2001; Cocke et al. 2005).

131 However, burned area estimation of small agricultural fires is understudied
132 relative to that for wildfires and remains challenging for several reasons. First, the
133 drawdown in greenness attributed to fires can be conflated with harvest (Hall et al.
134 2016). The NBR of pre-harvest pixels are higher than post-harvest pixels, because the
135 removal of biomass during harvest decreases NBR, which is dependent on vegetation
136 greenness. Second, scene availability is limited by cloud cover and haze contamination
137 and low temporal resolution. Because pairs of pre-fire and post-fire scenes are usually
138 required, the acquisition timing of scenes is critical: NBR estimated from different crop
139 stages between pre-harvest, post-harvest, and crop residue burning can affect
140 classification. Third, unlike forest fires, which can burn continuously for days over a
141 large area, agricultural fires are relatively small, short lasting, and vary spatially and

142 temporally year-to-year based on the timing of harvest (Thumaty et al. 2015). Fourth,
143 despite severe underestimation of burned area in croplands, it is also inaccurate to
144 assume that for example, entire 500 m x 500 m MCD64A1 pixels are fully burned.
145 Thus, simple land cover type-based correction factors (Zhu et al. 2017) may be
146 insufficient without considering burn heterogeneity at higher spatial resolution.

147 Fusion MODIS-Landsat (or hybrid moderate-high resolution sensor) techniques
148 have been developed to increase the spatial resolution of burned area mapping (e.g.
149 Loboda et al. 2007; Boschetti et al. 2015). Many of these studies rely on statistical
150 methods for land change detection and/or active fire ‘hotspot’ detections as an input
151 dataset for burn scar classification. (e.g. Loboda et al. 2007; Boschetti et al. 2015; Oliva
152 and Schroeder 2015). In the absence of extensive ground truth data, we use MCD64A1,
153 which integrates MODIS active fires into its land change detection-based burn scar
154 algorithm (Giglio et al. 2009), as a reference and training dataset for establishing NBR-
155 based thresholds and downscaling MODIS-scale burned area to Landsat resolution.

156 In this study, we develop a statistical two-tailed NBR algorithm using MODIS
157 and Landsat imagery in Google Earth Engine (Gorelick et al. 2017) to rapidly classify
158 post-monsoon (October to November) agricultural burned area in northwestern India
159 (Punjab and Haryana) from 2003-2016. The two-tailed NBR method is a two-step
160 classification based on thresholds for the pre-fire NBR_{max} and post-fire NBR_{min}
161 composites of each post-monsoon burning season. The two thresholds are derived from
162 the quantile-based intersection and separation of NBR_{min} and NBR_{max} distributions,
163 respectively, for burned and unburned agricultural areas. We compare ModL2T-derived
164 burned area (BA_{ModL2T}) to MCD64A1 and validate BA_{ModL2T} with independent
165 household survey results. In addition, we assess BA_{ModL2T} in the context of two different
166 crop residue burning practices, policy changes, mechanisation (use of combine
167 harvesters) and land fragmentation.

168 **2. Data and Methods**

169 **2.1. Study area**

170 The study area consists of two neighbouring agricultural states, Haryana (area: 44 119
171 km², 2011 population: 25.4 million) and Punjab (area: 50 427 km², 2011 population:
172 27.7 million), in northwestern India (Figure 2; <http://www.censusindia.gov.in/>).
173 Because Punjab and Haryana are situated at the heart of India’s ‘bread basket’, where
174 most farmers predominantly follow a rice (*kharif*)-wheat (*rabi*) rotation, this region is
175 an ideal area to perform high resolution analysis of burned area from small fires. For
176 our analysis, we exclude Chandigarh, an urban union territory and the capital of Punjab
177 and Haryana.

178 [FIGURE 2]

179 **2.2. Satellite data sources**

180 The datasets used in this study are primarily derived from Landsat and MODIS (Table
181 S1). We primarily use Google Earth Engine (GEE) to retrieve MODIS and Landsat
182 datasets and for geospatial analysis. GEE is a cost-free, petabyte-scale cloud computing
183 platform, which has been available since 2015 (Gorelick et al. 2017). All MODIS-
184 derived products used in the burned area algorithm and assessments are from the

185 Collection 6 (C6) suite. MCD64A1 C6, which replaced MODIS C5 with C6 active fires
186 and surface reflectance products as inputs, improved on small burn scars and omission
187 errors (Giglio et al. 2016).

188 *2.2.1 Double crop-fire cycle*

189 We first characterise the seasonal and diurnal temporal distributions of fires in
190 northwestern India. Following Vadrevu et al. (2011), we use the 1-km combined
191 MODIS/Terra and Aqua active fire counts (MCD14ML) to show the average annual
192 distribution of fires from 2003-2016. We also complement the fires with median NBR,
193 estimated from MODIS MOD09A1 8-day composite surface reflectance (SR) to show
194 variations in greenness in the rice-wheat double cropping system of northwestern India.
195 Giglio (2007) estimates an afternoon peak fire energy of 4.30 pm in central India based
196 on Visible and Infrared Scanner (VIRS) active fires. Central India primarily consists of
197 croplands with major *kharif* rice-growing areas (Mahajan et al. 2017). Vadrevu et al.
198 (2011) use the MODIS Terra/Aqua Fire Radiative Power (FRP) ratio to estimate a post-
199 monsoon peak fire energy of ~2.12 pm in Punjab. GFEDv4s also estimates the 3-hourly
200 diurnal cycle of fire emissions based on active fire observations from the Geostationary
201 Operational Environmental Satellite (GOES) Wildfire Automated Biomass Burning
202 Algorithm (WFABBA) (Mu et al. 2011).

203 ***2.3. The ModL2T algorithm for high-resolution burned area classification***

204 *2.3.1 Burned area estimation*

205 Previous studies on high-resolution agricultural burned area estimation in northwestern
206 India are generally constrained to 1-2 years of study (e.g. PRSC 2015; Yadav et al.,
207 2014a; 2014b). Here, we use GEE to expand the study time period to 14 years and
208 estimate post-monsoon agricultural burned area from 2003-2016. The post-monsoon
209 burning season is defined as October 1 to November 30. Figure 3 describes the
210 workflow for the ModL2T algorithm in GEE. The ModL2T algorithm can be
211 summarised as follows: (1) pre-process individual scenes; (2) composite cloud-free
212 scenes in pre-fire and post-fire collections; (3) define two-tailed thresholds based on the
213 quantile intersection of NBR in burned and unburned agricultural areas; (4) separately
214 derive MODIS and Landsat burned area; (5) merge Landsat and MODIS classifications
215 and apply agricultural mask.

216 Our method is primarily based on the MODIS MCD64A1 global burn mapping
217 algorithm and GFEDv4s small fires boost approach (Giglio et al. 2009; Randerson et al.
218 2012). We integrate moderate and high-resolution classification of seasonal fires in one
219 region and land cover type: croplands in northwestern India. MCD64A1 uses dynamic
220 NBR-based thresholds, based on 1-km MODIS active fire detections for selecting
221 burned and unburned training pixels, and is validated with Landsat-derived burned area
222 maps (Giglio et al. 2009). Here we use MCD64A1 as a training dataset due to the lack
223 of extensive ground data and remotely-sensed fire datasets at higher spatial resolution
224 for the duration of the study period and extent of the study region. In addition, we find
225 that Landsat images are too low in spatial resolution for visual interpretation, or to
226 definitively separate bare soil and burned fields and therefore obtain burned and
227 unburned training samples. While the Google Earth collection of DigitalGlobe and
228 CNES/Airbus imagery at sub-meter to meter resolution are viable for visual
229 interpretation, publicly available historical images are limited, often acquired outside

230 the post-monsoon period. Consequently, ModL2T adapts the MCD64A1 algorithm for
231 use with Landsat imagery in GEE. We improve on “baseline” MCD64A1 burned area
232 estimation with a Landsat-driven small fire boost – similar to the GFEDv4s approach of
233 using active fires to boost MCD64A1 – that increases the spatial resolution (500 m to 30
234 m) but decreases the temporal resolution (daily to bimonthly) of MCD64A1.

235 [FIGURE 3]

236 We use the near infrared and shortwave infrared SR bands from MODIS/Terra
237 (MOD09A1) and Landsat 5 (TM), 7 (ETM+), and 8 (OLI/TIRS) SR products to
238 estimate NBR (Tables S1, S2). We use MODIS/Terra daily surface reflectance rather
239 than that of Aqua, because the local daytime overpass time of the MODIS/Terra (10.30
240 am) – that of the MODIS/Aqua is 1.30 pm – is comparable with that of Landsat (10.00
241 am ± 15 minutes). MOD09A1 is a gridded Level-3, validated stage 2 product that
242 selects the best quality pixel over every 8-day period based on several criteria: cloud
243 cover, observation coverage, low-view angle and aerosol loading (Vermote et al. 2008).

244 While available MODIS/Terra and Landsat 7 scenes cover the study area for all
245 years from 2003-2016, Landsat 5 scenes only cover 2003-2010 and Landsat 8 scenes
246 from 2013-2016. We do not gap-fill Landsat 7 scan line errors and account for such
247 pixels as ‘no data’. We only consider pixels as marked ‘clear’ by quality flags. Cloud-
248 contaminated pixels are additionally filtered using the normalised difference of the
249 SWIR and Red bands, based on Xiang et al. (2013). Visible bands are more sensitive to
250 cloud contamination than SWIR bands; pixels where the SWIR SR exceeds Red SR are
251 retained:

$$252 \quad \frac{\rho_{SWIR} - \rho_{Red}}{\rho_{SWIR} + \rho_{Red}} > 0 \quad (2)$$

253 Burned area from MODIS and Landsat is separately derived from NBR due to
254 possible errors from differences in spatial resolution (500 m versus 30 m). Based on
255 Vadrevu et al. (2011), we leverage knowledge of the timing of the *khariif* rice crop and
256 fire activity patterns in Punjab and Haryana to define time brackets for pre-fire and
257 post-fire image collections. MODIS and Landsat NBR_{max} (maximum NBR composite
258 from pre-fire image collection: August 1 to September 30) and NBR_{min} (minimum NBR
259 composite from post-fire image collection: October 1 to November 30) images serve as
260 the two classification criteria of burned area on the basis that agricultural burned area
261 generally have high NBR_{max} (pre-fire) and low NBR_{min} (post-fire). For croplands, the
262 drawdown in greenness from burning can be conflated with harvest, so the drop in NBR
263 is not as abrupt as wildfires. However, burned vegetation and ash exhibit a more
264 negative difference between NIR and SWIR SR (or lower NBR) than bare soil and
265 stubble (Lewis et al. 2011; Pleniou and Koutsias 2013; Wang et al. 2018). Thus, we
266 expect NBR_{min} for burned fields to be lower than for unburned (fallow) fields.

267 The NBR_{max} and NBR_{min} thresholds are determined from the quantile-based
268 separation of NBR_{max} and NBR_{min} distributions of burned and unburned agricultural
269 areas, based on MODIS MCD64A1 burned area (500 m) and the ‘cultivated land’ class
270 from the GlobeLand30 land cover map for 2010 (Table S1). GlobeLand30 is a global
271 30-m, 10-class land cover map derived from > 20,000 Landsat and Chinese HJ-1
272 satellite images (Chen et al. 2014; Chen et al. 2017; globallandcover.com). According
273 to the University of Maryland MODIS-derived land cover classification (MCD12Q1,
274 C5.1) from 2001-2013, cropland area does not vary significantly (standard deviation of
275 ~1%) from year to year in the study region. We define the two-tailed classification

276 thresholds as the average composite MODIS NBR (NBR_{\min} or NBR_{\max}) at the quantile-
 277 based intersection of the τ percentile of MCD64A1-burned NBR and $1 - \tau$ percentile of
 278 unburned NBR:

$$279 \quad T = \frac{1}{2} [Q_{f(X)}(\tau) + Q_{f(Y)}(1 - \tau)] \quad (3)$$

280 where T is the NBR_{\max} or NBR_{\min} threshold, $Q(\tau)$ is the quantile function at τ percentile
 281 of the probability density function, f , of the distribution of NBR_{\min} or NBR_{\max} at burned
 282 (X) and unburned (Y) agricultural areas. This approach attempts to balance omission and
 283 commission errors. T_{\max} ranges from 0.635 to 0.706, and T_{\min} ranges from -0.057 to -
 284 0.014. Figure 4 shows an example of derived T_{\min} and T_{\max} for 2016. The quantile-based
 285 thresholds are generally located around $\tau = 0.71$ for T_{\min} and $\tau = 0.29$ for T_{\max} . This
 286 indicates that 71% unburned and burned agricultural areas are on average separated for
 287 each threshold. We also test the sensitivity of T_{\min} and T_{\max} using VIIRS active fire
 288 geolocations, over 2012-2017, as an independent training dataset: we find that VIIRS-
 289 trained T_{\min} and T_{\max} on average differ by +0.01 and -0.04, respectively, from
 290 MCD64A1-trained NBR thresholds, and achieve on average 61% and 65% of
 291 separability for NBR_{\min} and NBR_{\max} distributions, respectively. These small differences
 292 suggest that despite its coarser resolution, MCD64A1 can train T_{\min} and T_{\max} as well as
 293 VIIRS due to saturation in separability.

294 We use the MODIS-derived thresholds T_{\max} and T_{\min} on Landsat NBR_{\max} and
 295 NBR_{\min} , because MCD64A1 (500 m) is relatively coarse compared to Landsat
 296 resolution. Sensor-specific differences in spectral band wavelengths and the lack of
 297 Landsat availability can also introduce bias (Table S2, Figure S1). Thus, before deriving
 298 burned area from Landsat imagery, we correct for bias in Landsat NBR composites by
 299 adding the yearly regionally-averaged differences in MODIS and resampled Landsat
 300 NBR to Landsat NBR for all Landsat platforms. The compensation for Landsat NBR_{\max}
 301 ranges from 0.012 to 0.114, and that for NBR_{\min} ranges from -0.073 to 0.012. In this
 302 step, we also combine the MODIS-derived burned area with $BA_{MCD64A1}$ to minimize
 303 omission error generated by differences in the MCD64A1 and ModL2T algorithms.

304 [FIGURE 4]

305 Next, to merge the separately derived MODIS and Landsat classified burned
 306 area, we ‘carve’ out moderate-resolution MODIS burned pixels with high-resolution
 307 Landsat burned pixels (Figure S1). That is, we are more confident in Landsat to
 308 distinguish between burned and unburned fields, whereas MODIS more severely
 309 homogenizes large aggregates of individual landholdings due to its coarser spatial
 310 resolution. However, due to Landsat’s coarse temporal resolution, we are not confident
 311 in Landsat to accurately capture the highest NBR_{\max} and lowest NBR_{\min} when its usable
 312 data availability is temporally-sparse and/or biased. Thus, we first create a criterion to
 313 mask such areas. After resampling to MODIS resolution, Landsat NBR_{\min} and NBR_{\max}
 314 that deviate more than ± 0.1 from MODIS NBR_{\min} or NBR_{\max} are masked. With this
 315 criterion, Landsat NBR_{\min} and NBR_{\max} must approximately agree with those of MODIS
 316 for the ~ 238 Landsat burned and unburned pixels to take precedent and replace a
 317 MODIS pixel. The NBR absolute difference threshold of 0.1 allows for some variance
 318 for composites of best quality Landsat pixels from different acquisition dates and
 319 sensor-specific differences in spectral band wavelengths (Table S2). While 0.1 is an
 320 arbitrary selection, a large departure of Landsat from MODIS NBR indicates that pixels
 321 of available Landsat scenes are generally cloudy and/or do not capture scenes near peak

322 monsoon growing season (NBR_{max}) and/or in the post-burning (NBR_{min}) period when
323 the burn scar is still visible. Furthermore, it may be the case that there are some Landsat
324 observations in the two-month windows for the pre-fire and post-fire collections, but the
325 acquisition dates of ‘best quality’ Landsat pixels may not be close to that for MODIS
326 pixels. In the last step, we apply an agricultural mask based on GlobeLand30 land
327 cover. The final ModL2T-derived burned area (BA_{ModL2T}) is an estimate of the total
328 post-monsoon agricultural burned area at the Landsat 30-m resolution.

329 We also assign confidence scores to BA_{ModL2T} on a pixel-by-pixel basis by
330 designating different categorical values to burned area derived from MCD64A1,
331 Landsat-only ModL2T, and MODIS (MOD09A1)-only ModL2T. We are most
332 confident in MCD64A1 and least confident in MODIS-only ModL2T, so we assign
333 $BA_{MCD64A1}$ a value of 3, Landsat-only BA_{ModL2T} a value of 2, and MODIS-only
334 BA_{ModL2T} a value of 1. Adding these burned area layers together yields a confidence
335 scale from 1 (low) to 6 (high) (Table S4).

336 2.3.2. MCD64A1-based geographical accuracy assessment

337 We use MCD64A1 as the reference dataset in a geographic accuracy assessment of the
338 two-tailed threshold burned area classification algorithm. Here, we compare MCD64A1
339 with MODIS (MOD09A1)-only BA_{ModL2T} in order to evaluate the burned area
340 classification algorithms on a pixel-by-pixel basis at the MODIS 500-m resolution. We
341 estimate Cohen’s kappa coefficient (κ), which evaluates the agreement between the
342 reference and test classification after random chance is removed (Cohen 1960).

343 2.3.3. Validation using household survey results

344 We validate BA_{ModL2T} by using a 2016 survey on farm management practices across the
345 IGP. The 2016 survey data asks participants about burning crop residue in the post-
346 monsoon (Did you burn crop residue before planting wheat?) and includes GPS
347 coordinates. Because the survey responses inherently distinguish between burned versus
348 unburned fields, this validation addresses the conflation of burning versus harvest. We
349 use 1111 responses from farmers in 30 Punjab and 32 Haryana villages. However, the
350 GPS coordinates are located not in-field, so we cannot match responses to individual
351 fields. We therefore group responses by village name and match mean GPS coordinates
352 with an accuracy < 10 m to the village shapefiles. On average, 18 ± 5 households were
353 surveyed per village. We normalise the % households that burn crop residue with
354 landholding area by village in post-monsoon 2016. For comparison, we estimate the %
355 BA_{ModL2T} of total village cultivated area based on GlobeLand30. Due to these
356 normalised approximations spurred by data limitations, the two metrics of % burning
357 per village are not comparable in absolute terms.

358 2.3.4. Further assessments of ModL2T-derived burned area

359 In lieu of a single ‘ground truth’ validation, we further assess BA_{ModL2T} with simple
360 checks using: (1) pixel-level (active fire locations), (2) district-level (previous burned
361 area estimates) and (3) region-level (satellite aerosol optical depth, AOD). We consider
362 $p < 0.01$ to be statistically significant.

363 **Assessment 1 (VIIRS active fire locations):** The GFEDv4s small fires boost approach
364 uses the ratio of dNBR at active fire locations outside and inside burned areas

365 (Randerson et al. 2012; van der Werf et al. 2017). In line with this approach based on
366 the co-location of fires and burned area, we use higher spatial resolution (375 m)
367 Visible Infrared Imaging Radiometer Suite (VIIRS) active fire geolocations
368 (VNP14IMGML, Collection 1) over October and November in 2012-2016 to assess
369 omission errors. We consider daytime VIIRS active fire detections classified as
370 'presumed vegetation fire' (Giglio 2015). This assessment is based on the fraction of
371 VIIRS active fires co-located within the classified burned area; a higher fraction
372 indicates a lower omission error. BA_{ModL2T} and $BA_{MCD64A1}$ are first resampled to 1 km
373 to account for off-nadir MODIS and VIIRS pixel area.

374 **Assessment 2 (previous burned area estimates):** We compare post-monsoon district-
375 level BA_{ModL2T} to that of PRSC (2015) and Yadav et al. (2014a; 2014b). PRSC (2015)
376 estimated district-level burned area from post-monsoon burning in Punjab in 2014 and
377 2015 by performing classification on multi-date Normalised Difference Vegetation
378 Index (NDVI) from high-resolution multi-sensor (Landsat 8, AWiFS and LISS-3)
379 satellite imagery from October 15 to November 15. Yadav et al. (2014a; 2014b) used
380 the Iterative Self-Organising Data Analysis (ISODATA) clustering classifier in multi-
381 date unsupervised classification of AWiFS satellite-derived NDVI images to estimate
382 agricultural burned area in ten districts (Ambala, Faridabad, Jind, Kaithal, Karnal,
383 Kurukshetra, Panipat, Sirsa, Sonipat and Yamunanagar) in northern Haryana in 2013
384 and three districts (Kaithal, Karnal and Kurukshetra) in 2010, respectively. PRSC
385 (2015) and Yadav et al. (2014a; 2014b) validated district-level burned area
386 classifications using ground truth GPS points and/or field photographs.

387 **Assessment 3 (MODIS AOD):** Aerosol optical depth (AOD) represents the column-
388 integrated aerosol loading and measures the extinction of solar radiation. High AOD
389 values represent hazy conditions and generally poor air quality. We use Level-2 AOD
390 product from MODIS/Terra, operationally available at 3 km and 10 km pixel resolution,
391 to assess detrended correlation with BA_{ModL2T} (Table S1). Mid-visible AOD retrievals at
392 $0.55 \mu\text{m}$ are used in this study. The Level-2 AOD retrievals are available on a daily
393 basis, which were then uniformly gridded to produce a per-pixel AOD mean spatial
394 distribution at 3×3 km and 10×10 km grid cells, for Punjab and Haryana. The data
395 were then averaged for each post-monsoon period from 2003-2016. For the 10 km AOD
396 retrieval, we use the combined Dark-Target (DT) and Deep-Blue (DB) product, which
397 merges aerosol retrievals over both dark vegetated and bright reflecting regions (e.g.
398 arid/desert areas except snow surface) (Singh et al. 2017). In terms of accuracy of the 10
399 km product, the expected error envelope is reported to be $\pm(0.05 + 0.15\tau)$ over land
400 (Levy et al. 2013) for DT retrievals and $\pm(0.03 + 0.2\tau)$ for DB retrievals (Sayer et al.
401 2013), where τ represents AOD. This combined DT/DB product uses NDVI climatology
402 for differentiating between dark and bright land areas. In this study, we use the best-
403 quality retrievals of the combined DT/DB AOD data (for only quality flag = 3
404 retrievals). Additionally, the 3 km AOD retrievals are also used to analyse spatial
405 distribution of aerosol loading at a higher resolution and study relationship with burned
406 area. The 3 km AOD data are based on DT retrievals, limited to vegetated pixels, which
407 cover the majority of Punjab and Haryana. The uncertainty of the 3 km AOD retrieval is
408 reported as $\pm(0.05 + 0.15\tau)$ (Munchak et al. 2013), where τ represents AOD.

409 **2.4 Landholdings and combine harvesters**

410 We consider ancillary data in landholding size and combine harvester use to assess
411 trends in farm fragmentation and mechanisation. The Agricultural Census division of

412 Indian Department of Agriculture, Cooperation, and Farmers Welfare conducts the
413 Agricultural Census in India (<http://agcensus.nic.in/>) and provides two online databases:
414 Agricultural Census and Input Survey. The online database of the Agricultural Census,
415 which is based on census and input sample survey, contains quinquennial data regarding
416 the number, average size and area of landholdings by country, state, district and tehsil
417 (sub-district) and by social group (caste, tribe) and gender from 1995-96 to 2010-11
418 (<http://agcensus.dacnet.nic.in/>). The Input Survey is another online database with
419 quinquennial data of detailed information about agricultural implements and machinery,
420 including total combine harvesters by landholding size, from 1996-97 to 2011-12
421 (<http://inputsurvey.dacnet.nic.in/>). The 2016 household survey also asks participants
422 about harvest methods (How do you harvest your rice crop?). The possible response
423 choices are: (1) fully mechanical (e.g. combine harvester), (2) partially mechanical (e.g.
424 thresher), (3) manually, (4) both manual and mechanical, (5) other and (6) never
425 harvested rice. We use all responses from farmers in Punjab and Haryana to assess the
426 relationship between combine harvester use and rice residue burning before sowing
427 wheat.

428 **2.5. Methods of crop residue burning**

429 In a field visit, Kumar et al. (2015) identified two dominant crop residue burning
430 practices in Punjab: (1) whole field burning and (2) partial burning (small stalks). We
431 use Google Earth's collection of fine-resolution imagery (DigitalGlobe and CNES/
432 Airbus) to qualitatively characterise crop residue burning practices (e.g. whole field,
433 partial field burning) at the resolution of individual fields in Punjab and Haryana. We
434 discuss the differences in scarring from and spatial distribution of the two dominant
435 burning practices. Most scenes assessed were acquired in 2014-2016.

436 **3. Results**

437 **3.1. Spatio-temporal distributions in fire activity**

438 Figure 5(a) shows the average annual timing of the bimodal fire activity and the double-
439 crop system in northwestern India. Whereas high NBR represents high vegetation cover
440 (peak greenness) during the monsoon and winter crop growing seasons, low NBR
441 represents low vegetation cover (bare soil, burn scars) after harvest and crop residue
442 burning. MCD64A1 burn frequency shows repeated post-monsoon fire activity from
443 2003-2016, particularly in southern-central Punjab (Figure 5(b)), where fires tend to
444 occur later in the fire season than in parts of northern Punjab (Figure 5(c)). In addition,
445 Aqua (1.30 pm local time) averages 645 ± 289 % higher in fire counts than Terra (10.30
446 am local time) during the 2003-2016 post-monsoon burning seasons, which is consistent
447 with the afternoon peak fire energy (4.30 pm local time) estimated by Giglio (2007).
448 Estimates from 3-hourly GFEDv4s, based on Mu et al. (2011), and Vadrevu et al.
449 (2011) point to an earlier (~ 2.12 pm local time) post-monsoon peak fire energy in
450 Punjab (Figure S3). However, Vadrevu et al. (2011) is limited by MODIS Terra/Aqua
451 overpass times, and Mu et al. (2011) use land cover type matching to broadly attribute
452 normalised fire diurnal cycles globally based on GEOS observations in North and South
453 America.

454

[FIGURE 5]

455 **3.2. ModL2T-derived burned area**

456 **3.2.1. Comparison to MCD64A1 burned area estimates**

457 The strength of agreement (Cohen's κ) between $BA_{MCD64A1}$ and MODIS-only BA_{ModL2T}
458 is consistent and ranges from 0.4-0.53 (moderate) (Landis and Koch 1977). Overall
459 accuracy ranges from 82-89%. ModL2T averages $66 \pm 31\%$ higher post-monsoon
460 burned area than MCD64A1 in Punjab and Haryana from 2003-2016 (Figure 6, Table
461 S3). We estimate 49-72% of BA_{ModL2T} with good confidence (score ≥ 3) (Figure S2). In
462 terms of BA_{ModL2T} in excess of $BA_{MCD64A1}$, Landsat-only BA_{ModL2T} (33%, score = 2)
463 generally dominates MODIS-only BA_{ModL2T} (6%, score = 1). BA_{ModL2T} in 2003-07 and
464 2011-12 may be less accurate as a result of relatively low availability of usable and
465 cloud-free data for MODIS and/or Landsat (Figures S1, S2). Proportionally, $BA_{MCD64A1}$
466 in Haryana constitutes a smaller fraction ($14 \pm 3\%$) of total burned area in the study
467 region than BA_{ModL2T} ($24 \pm 3\%$). This indicates that the ModL2T increase in burned
468 area over MCD64A1 is partly driven by its additional burn scar detections in Haryana.

469 [FIGURE 6]

470 **3.2.2. Validation with 2016 household survey**

471 Figure 7(a) shows the spatial comparison between $BA_{MCD64A1}$ and MODIS-only
472 BA_{ModL2T} in 2016. The overall accuracy is 84% with moderate agreement ($\kappa = 0.53$)
473 (Table 1). Disagreements between $BA_{MCD64A1}$ and MODIS-only BA_{ModL2T} mainly lie in
474 central Haryana and northern Punjab.

475 [FIGURE 7]

476 [TABLE 1]

477 We validate BA_{ModL2T} with independent household survey results from 2016.
478 We compare post-monsoon village-level survey crop residue burning rates, normalised
479 by landholding size, with BA_{ModL2T} expressed as a fraction of cropland area. The
480 village-level fraction of surveyed households that burn crop residue is moderately
481 correlated with fractional BA_{ModL2T} ($r = 0.62, p < 0.01$) (Figure 8(a)). In contrast,
482 $BA_{MCD64A1}$ achieves a weaker correlation of $r = 0.54$ ($p < 0.01$) and tends to cluster at
483 fractions burned of 0 or 1, likely due to its moderate spatial resolution (Figure 8(b)).
484 $BA_{MCD64A1}$ and BA_{ModL2T} explain 28% and 37% of variability (adjusted R^2) in survey
485 burn rates, respectively, indicating that BA_{ModL2T} is better able to capture variability in
486 the 'ground truth' burn rates.

487 [FIGURE 8]

488 **3.2.3. Additional assessments of BA_{ModL2T} and $BA_{MCD64A1}$**

489 We first assess omission error based on the fraction of VIIRS active fire detections co-
490 located with $BA_{MCD64A1}$ and BA_{ModL2T} , during the 2012-2016 post-monsoon burning
491 seasons. With a higher spatial resolution (375 m) than MODIS/Terra and Aqua (1 km),
492 VIIRS is able to more consistently detect smaller and cooler fires (Figure S4). We find
493 that BA_{ModL2T} and $BA_{MCD64A1}$, resampled to 1 km, are co-located with 95-100% (0-5%
494 omission error) and 69-76% (24-31% omission error), respectively, of VIIRS-detected
495 active fires within cropland areas (Table S5). The maximum commission error is
496 slightly higher for BA_{ModL2T} (18-23%) than $BA_{MCD64A1}$ (13-17%) but may reflect

497 undetected active fires outside VIIRS overpasses or obscured by thick haze or clouds. In
498 particular, $BA_{MCD64A1}$ is often unable to detect active fire hotspots in regions of
499 periphery burning and scattered fires, such as in central Haryana and northern Punjab
500 (Figures 6, S4). Over the 5-year period from 2012-2016, VIIRS detected active fires in
501 73% of the $0.03^\circ \times 0.03^\circ$ grid cells in Punjab and Haryana, while MODIS only detected
502 active fires in 61% of the area (Figure S4c). In addition, VIIRS detected that 51% of
503 grid cells burned consecutively during post-monsoon from 2012-2016, while MODIS
504 detected only 31% of grid cells by this criterion.

505 Next, we compare district-level burned area from previous estimates (PRSC
506 2015; Yadav et al. 2014a; 2014b) to BA_{ModL2T} . Total Punjab BA_{ModL2T} is 5% lower and
507 18% higher than that of PRSC (2015) in 2014 and 2015, respectively. In contrast,
508 Punjab $BA_{MCD64A1}$ is lower than PRSC (2015) burned area estimates in both 2014 and
509 2015 by 20% and 3%, respectively (Figure S5). However, for northern Haryana
510 districts, $ModL2T$ and $MCD64A1$ both tend to overestimate burned area relative to
511 Yadav et al. (2014a; 2014b). District-level BA_{ModL2T} ($r = 0.88, p < 0.01$) and $BA_{MCD64A1}$
512 ($r = 0.87, p < 0.01$) are strongly correlated with PRSC (2015 and Yadav et al. (2014a;
513 2014b) burned area estimates. In terms of mean absolute error, $ModL2T$ (257 km^2)
514 outperforms $MCD64A1$ (279 km^2). However, $MCD64A1$ (slope = 1.03 ± 0.08) shows
515 less overall bias than $ModL2T$ (slope = 0.93 ± 0.07), which tends to overestimate
516 burned area in Haryana districts relative to Yadav et al. (2014a; 2014b).

517 Finally, we assess 14-year trends and detrended interannual variations in mean
518 post-monsoon MODIS AOD and BA_{ModL2T} . We find increased aerosol loading in
519 ground-based column AOD measurements, during October-November, from the
520 Aerosol Robotic Network (AERONET) site at Lahore (in the neighbouring Pakistan
521 province of Punjab) (Figure S6). Previous work of using HYSPLIT trajectories with
522 MODIS FRP suggests that AOD weakly and positively co-varies with fire intensity
523 during post-monsoon (Liu et al. 2018). Due to potential long-range atmospheric
524 transport of aerosols from the fire source region, we consider trends and interannual
525 variability at coarse spatial scale. In the 14-year time span, satellite AOD increased by
526 $0.017 \pm 0.003 \text{ yr}^{-1}$ ($p < 0.01$) and BA_{ModL2T} by $713 \pm 115 \text{ km}^2 \text{ yr}^{-1}$ ($p < 0.01$) (Figure
527 S7a-b). While increased Landsat scene availability (Figure S1) may account for the
528 some of the upward trend in BA_{ModL2T} , the upward trend in $BA_{MCD64A1}$, which has no
529 dependency on Landsat, is higher at $966 \pm 84 \text{ km}^2 \text{ yr}^{-1}$ ($p < 0.01$) (Figure S7a).
530 Additionally, regional BA_{ModL2T} is weakly positively correlated with mean regional
531 AOD for both the 3 km ($r = 0.39, p = 0.17$) and 10 km ($r = 0.36, p = 0.21$) datasets, but
532 not statistically significant at the 99% significance level (Figure S7c). Comparatively,
533 $BA_{MCD64A1}$ is anti-correlated with mean regional AOD (3 km AOD: $r = -0.43, p = 0.13$;
534 10 km AOD: $r = -0.54, p < 0.05$) (Figure S7d).

535 3.3. Trends in landholding size and combine harvesters

536 The median landholding size in Haryana (1-2 ha) is smaller than that of Punjab (2-3 ha);
537 only ~0.5% of landholdings in Haryana and ~1% in Punjab are over 20 ha (Figure 9).
538 After some consolidation of small landholdings from 1995-96 to 2000-01, landholdings
539 were increasingly fragmented from 2000-01 to 2010-11. Landholdings smaller than 7.5
540 ha increased from 88.2% to 89.5% of total landholdings in Haryana and 75.4% to
541 77.1% in Punjab from 2000-01 to 2010-11. Simultaneously, the number of combine
542 harvesters tabulated by the Indian Input Survey increased 20-fold from 14 664 in 1996-
543 97 to 297 132 in 2011-12 in Haryana and almost 3-fold from 93 191 in 1996-97 to 256

544 162 in 2011-12 in Punjab. In the 2016 household survey, 68% of surveyed farmers that
545 used a combine harvester to harvest rice subsequently burned the crop residue in
546 preparation for sowing wheat in Punjab and Haryana. Of those who burned crop
547 residue, 93% used fully or partially mechanical methods of harvesting.

548 [FIGURE 9]

549 **3.4. Two burning practices: size and shape of burn scars**

550 Based on fine-resolution DigitalGlobe and CNES/Airbus historical imagery in
551 November 2016, we observe two dominant crop residue burning practices in the study
552 region that Kumar et al. (2015) observed in a field visit in Punjab: burning of (1) whole
553 fields and (2) piled-up loose residue at the centre of fields (Figure 10). Although
554 farmers in Punjab and Haryana seem to employ a mixture of the two burning practices,
555 available DigitalGlobe and CNES/ Airbus images of the study region suggest that
556 farmers in Punjab tend to fully burn fields and some Haryana farmers partially burn
557 fields post-harvest. Kumar et al. (2015) also concluded that whole-field burning is more
558 popular in practice than partial burning in Punjab. Whole field burning induces dark
559 scarring of entire fields such that adjoining fields burned in this way within days of each
560 other are starkly contrasted against the surrounding unburned landscape (Figure 10(a-
561 b)). In contrast, partial burning leaves circular or ring-shaped scarring in the centre of
562 fields; only ~1/9 of the field area is in fact scarred (Figure 10(c-d)).

563 [FIGURE 10]

564 **4. Discussion**

565 **4.1. ModL2T-derived burned area: validation, assessments, and uncertainties**

566 In this study, we use MODIS and Landsat imagery to estimate post-monsoon
567 agricultural burned area in northwestern India for 14 years from 2003-2016. Use of
568 Landsat imagery has been primarily limited by: (1) its low temporal resolution (16 days)
569 and (2) storage and computing power. To minimise these limitations, we implement a
570 hybrid MODIS-Landsat approach in Google Earth Engine, a cloud-computing platform
571 with petabyte-scale storage, to rapidly process large collections of MODIS and Landsat
572 imagery and expand the spatio-temporal range of study.

573 Here we aim to improve $BA_{MCD64A1}$ by extrapolating from the MCD64A1
574 training data, which we assume to be valid, and adding Landsat SR as an input. We
575 caution that use of MCD64A1 as a training dataset should be amended with availability
576 of ground data or fine-resolution multispectral imagery. Given this limitation, ModL2T
577 improves on MCD64A1 from the spatial resolution rather than the algorithm
578 perspective. The higher average contribution of Landsat-only BA_{ModL2T} (33%) over
579 MODIS-only BA_{ModL2T} (6%) to overall BA_{ModL2T} confirms that additional burned area
580 from ModL2T relative to MCD64A1 is primarily driven by integration of Landsat
581 imagery rather differences in the ModL2T and MCD64A1 algorithms.

582 In comparison to MCD64A1, the ModL2T algorithm estimates on average $66 \pm$
583 31% higher burned area in Haryana and Punjab during post-monsoon, from 2003-2016.
584 We validate the BA_{ModL2T} with survey data from 2016. The higher correlation ($r = 0.62$,
585 $p < 0.01$) between village-level fractions of households that burn crop residue,
586 normalised by landholding area, and BA_{ModL2T} , compared to $BA_{MCD64A1}$ ($r = 0.54$, $p <$

587 0.01), of total village cropland area suggests that the ModL2T algorithm can estimate
588 burned area with increased accuracy. According to this validation, both ModL2T and
589 MCD64A1 tend to underestimate burned area in northern Punjab villages and
590 overestimate that in northeastern Haryana villages. The homogenous definition of the
591 time range for pre-fire and post-fire collections for the ModL2T algorithm may have
592 restricted burned scar detection. For example, the northern Punjab districts of
593 Kapurthala and Jalandhar tend to burn earlier than other districts. Thus, more spatially
594 dynamic temporal specifications of the pre-fire and post-fire image collections and
595 detailed knowledge of the cropping patterns may decrease omission errors.

596 In additional assessments, we find that BA_{ModL2T} improves on $BA_{MCD64A1}$ in
597 terms of omission error, comparison with previous estimates of burned area, and
598 relationship with satellite AOD. First, we find that BA_{ModL2T} captures 95-100% of
599 VIIRS active fires within its extent, while $BA_{MCD64A1}$ is only co-located with 69-76% of
600 VIIRS active fires. Second, BA_{ModL2T} improves on $BA_{MCD64A1}$ in terms of mean
601 absolute error relative to previous district-level burned area estimates (PRSC 2015;
602 Yadav et al. 2014a; 2014b). The strong overall agreement ($r = 0.87-0.88$, $p < 0.01$) with
603 PRSC (2015) and Yadav et al. (2014a; 2014b) burned area suggests that the ModL2T
604 and MCD64A1 can achieve burned area estimates similar to methods using high-
605 resolution satellite imagery, supervised classification, and ground truth validation at the
606 district-level. While overall bias is higher in BA_{ModL2T} than $BA_{MCD64A1}$ relative to
607 previous estimates, the mean absolute error of BA_{ModL2T} is lower. Finally, we find
608 commensurate increasing trends in burned area and satellite AOD from 2003-2016,
609 suggesting increasing fire activity and hazier conditions over the region during post-
610 monsoon. Crop residue burning in Punjab and Haryana is a major source of regional
611 pollution and driver of satellite AOD variability during post-monsoon months,
612 influencing even aerosol properties and air quality of urban areas downwind
613 (Kaskaoutis et al., 2014; Liu et al. 2018). Similar to Liu et al. (2018), we find that
614 BA_{ModL2T} exhibits a weak positive correlation with satellite AOD, after detrending, in
615 contrast to the anti-correlation observed with $BA_{MCD64A1}$.

616 Of course, these validation and assessments are also subject to various
617 limitations and uncertainties. For example, the 2016 household survey is spatially
618 constrained to northeastern Haryana and northern Punjab and may be not representative
619 of entire villages, as some villages have a small sample size. Without in-field GPS data
620 and more detailed information on burn practices, we did not take into account partial
621 burning and assumed a field is entirely burned if a farmer affirms crop residue burning.
622 Similar to MODIS, VIIRS active fires are limited by satellite overpass times, the short
623 burn duration of agricultural fires, and cloud or thick haze obscuration of fires. Further,
624 by only using satellite imagery with high spatial resolution but low temporal resolution,
625 PRSC (2015) and Yadav et al. (2014a; 2014b) burned area estimations are more
626 susceptible to cloud and haze contamination and limited usable scenes. Finally, satellite
627 AOD can be influenced by other local and regional post-monsoon pollution sources,
628 such as urban and industrial emissions and Diwali festival fireworks (Cusworth et al.
629 2018). While the % valid pixels used for estimating mean regional AOD is relatively
630 consistent across years ($38 \pm 3\%$), Cusworth et al. (2018) found that the MODIS cloud
631 algorithm confuses thick haze with clouds, implying underestimation of AOD for days
632 with severe haze, as in November 2016.

633 *4.2. Limitations of burned area algorithms in northwestern India*

634 $BA_{MCD64A1}$, which the GFEDv4s fire emissions inventory relies on, is derived from
635 MODIS, a moderate-resolution satellite (500 m). In India, however, the average
636 landholding tends to be comparatively small and fragmented (Misri 1999). In Punjab
637 and Haryana, only 0.5-1% of landholdings are > 20 ha, comprising just 7-8.6% of total
638 area. Because prescribed agricultural burning is constrained by landholding size, the
639 estimation of small fire burned area is important in Punjab and Haryana. The Randerson
640 et al. (2012) and van der Werf et al. (2017) approach for estimating the small fires
641 contribution in GFEDv4s relies on two ratios: (1) FC_{out}/FC_{in} , or the ratio of active fires
642 outside to those inside the $BA_{MCD64A1}$ extent for each $0.25^\circ \times 0.25^\circ$ grid cell and (2)
643 $(dNBR_{out} - dNBR_{control})/(dNBR_{in} - dNBR_{control})$, or the ratio that represents the dNBR
644 outside and inside $BA_{MCD64A1}$ relative to an unburned control area. This methodology
645 assumes confidence in $BA_{MCD64A1}$ to be from more spatially expansive fires and a linear
646 correlation of burn severity with burned area (Randerson et al. 2012). However, unlike
647 wildfires, whose burn severity and burned area extent can vary greatly, cropland fires
648 are usually controlled in burn rate, time and area, thus limiting the upper bound of burn
649 severity and burned area extent per fire. For cropland fires, dNBR has been used more
650 as a threshold for burned area classification rather than a proxy for burn severity (e.g.
651 McCarty et al. 2008; 2009; Oliva and Schroeder 2015; Zhu et al. 2017). However, the
652 downward trajectory of NBR is influenced by both harvest and burning (Hall et al.
653 2016). Clearly attributing decreases in NBR to burning remains challenging due to noise
654 and gaps in NBR timeseries. In northwestern India, the time pressures of the double-
655 crop system force a quick harvest-to-sowing turnaround time during post-monsoon, so
656 burning may closely follow harvest (Kumar et al. 2015). Thus, the 16-day composite
657 MOD13A1 SR product may be too temporally coarse for cropland dNBR in that it
658 collects the best quality pixels and could miss the lowest NBR pixels immediately post-
659 fire.

660 Moreover, based on the two dominant types of burning practices (whole and
661 partial field burning) as seen in DigitalGlobe images of Punjab and Haryana during the
662 post-monsoon burning season, the method in which farmers burn piled up loose crop
663 residue in the centre of the field (particularly in Haryana) may be more difficult to
664 detect due to sub-landholding size fires. Of course, this difficulty is compounded by
665 small median landholding sizes in Haryana (1-2 ha) and Punjab (2-3 ha). Particularly in
666 Haryana, the potential prevalence of partial burning, in conjunction with small median
667 landholding size (1-2 ha), makes it more difficult for moderate-resolution satellites to
668 detect agricultural fires and accurately estimate burned area. The pile-up residue method
669 only burns the centre of fields (~1/9 of field area), leaving a centred ring-shaped mark,
670 while whole field burning blackens the entire field. Thus, if a GFED grid cell contains a
671 small sample of large or small fires, the dNBR ratio used in the small fire boost
672 algorithm may be inaccurate. Similarly, if no or little $BA_{MCD64A1}$ is present within a grid
673 cell, the potential of the small fires boost is limited. These challenges, some region-
674 specific, are reflected in the performance of the GFEDv4s small fires boost (Randerson
675 et al. 2012; van der Werf et al. 2017): added small fires emissions from 2003-2016
676 average ~20% of total post-monsoon Punjab and Haryana emissions, compared to ~47%
677 of annual global agricultural emissions.

678 Finally, GFEDv4s and MCD64A1, both of which use active fire detections, are
679 by extension susceptible to spatio-temporal limitations in MODIS satellite overpass
680 times and detection limit. In India, agricultural fires typically last no more than half an
681 hour (Thumaty et al. 2015). VIIRS, at a higher resolution (375 m), detected ~20% more

682 0.03° x 0.03° grid cells with active fires than MODIS/Terra and Aqua from 2012-2016.
683 Even so, VIIRS would not be able detect small and cool fires and fires below optically
684 hazy areas and outside of its overpass time. For example, if the peak fire energy is close
685 to the late afternoon time (4.30 pm local time) estimated by Giglio (2007), the earlier
686 daytime overpass times of MODIS/Terra and Aqua (10.30 am and 1.30 pm,
687 respectively) and VIIRS (1.30 pm) imply missed fire detections. Oliva and Schroeder
688 (2015) show that VIIRS-derived burned area compares poorly to a Landsat 8 reference
689 dataset; in north India, the VIIRS fire detection rate was only 7.75% for fires < 10 ha
690 and 28.82% for those > 10 ha.

691 Due to the short time window to detect burn scars and region-specific
692 limitations, namely landholding size and variations in burning practices, sub-weekly,
693 sub-Landsat resolution imagery is required to fine-tune burned area estimates at the
694 landholding level. The low temporal availability of Landsat increases its susceptibility
695 to low pixel availability from haze and clouds. Several scenes cover the study region,
696 and the mismatch in date acquired may cause incongruity if one scene is hazy and
697 cloudy. Further, although we use MOD09A1 (8-day composite) as the surface
698 reflectance product instead of MOD13A1 (16-day composite) used in Randerson et al.
699 (2012) and van der Werf et al. (2017), MOD09A1 may still be too coarse in temporal
700 resolution. Thus, the limited overpass frequency of available satellite imagery from
701 MODIS and Landsat suggests that the burned area estimates in this study are still likely
702 conservative.

703 ***4.3. Implications of groundwater policy, increasing mechanisation and land*** 704 ***fragmentation***

705 In 2009, the Punjab and Haryana governments implemented the ‘Preservation of Sub-
706 soil Water Act, 2009’ (Ordinance in 2008) to counteract groundwater depletion by
707 delaying rice transplanting to after June 10 and 15, respectively. In effect, this policy
708 forces the rice harvest season to extend to mid-November (Bhullar and Bhullar 2013;
709 Singh 2009; PRSC 2015). Based on the 2016 household survey, 76% of farmers in
710 Punjab and Haryana ideally prefer to sow wheat before November 15, but only 44%
711 were able to sow wheat before mid-November. This ideal-actual sow date difference is
712 starker for farmers who burned crop residue: 78% prefer to sow before mid-November,
713 but only 35% sowed before this date. We find an average step increase of ~28% in
714 BA_{ModL2T} from the 2003-07 to 2008-16 time period. A two-sample t-test shows that the
715 difference in BA_{ModL2T} between the two time periods is statistically significant ($p <$
716 0.01) with a mean difference of 5762 km² (95% CI: [3086, 8438] km²). However,
717 further work is needed to robustly quantify the effect of potential delays in rice harvests
718 and agricultural fires on a finer temporal scale, or daily to weekly basis.

719 In northwestern India, agricultural mechanisation, combined with the time-
720 intensive double-crop system, drives crop residue burning. Combine harvesters,
721 normalised by total landholdings, increased by 58% from 2001-02 to 2011-12.
722 However, at the same time, % landholdings < 7.5 ha increased by ~1.5% from 2000-01
723 to 2010-11 in Punjab and Haryana. Increasing land fragmentation may slow the rate of
724 agricultural mechanisation as marginal and small landholdings become too fragmented
725 to be mechanised or mechanised in the same way as medium and large landholdings
726 (Deininger et al. 2017; Mehta et al. 2014). Specifically, the widening technology gap
727 between marginal to small (manual and animal-drawn) and medium to large (tractor-
728 drawn and self-propelled) landholdings may be reduced through consolidation (Mehta

729 et al. 2014). However, if consolidation efforts strengthen as a result of the demand for
730 higher crop productivity and agricultural mechanisation, crop residue burning rates may
731 accelerate unless alternative, more sustainable methods become viable and cost-time
732 effective.

733 *4.4. Future directions for burned area mapping and fire emissions inventories*

734 The recent proliferation of finer resolution satellites, such as VIIRS (375 m, daily, post-
735 2012), Sentinel-2 (10-20 m, every 5 days, post-2015) and Planet (<5 m, daily, post-
736 2016), offers added potential for active fire and burn scar detection (Drusch et al. 2012;
737 Strauss 2017). Integration of these products with the hybrid MODIS-Landsat framework
738 can improve accuracy in burned area estimation and fire emissions inventories for more
739 recent years of study (e.g. Wang et al. 2017). For example, the emissions factor for
740 partial burning may be higher than whole field burning, but its burn scar is sub-
741 landholding size and its emissions footprint is therefore difficult to estimate even at
742 Landsat resolution. Fine-resolution sensors can be used to distinguish the spatial
743 patterns of the burning practices to better inform fire emissions inventories retroactively
744 and proactively. Additionally, the coupling of cloud computing and geospatial datasets
745 in GEE makes near-real time analysis possible for policy and management decisions
746 (Gorelick et al. 2017). Rapid availability of updated collections of satellite-derived
747 products on GEE can decrease the turnover time for new versions of fire emissions
748 inventories, such as GFEDv4s, which currently uses MCD64A1 C5.1 (van der Werf et
749 al. 2017). Finally, our reliance on MCD64A1 as a training dataset in the absence of a
750 spatio-temporally expansive ground truth dataset signals a need for collection of
751 detailed multi-year survey data on crop residue burning in northwestern India. Due to
752 high uncertainties associated with small cropland fires, we recommend that global
753 burned area and fire emissions datasets integrate ground truth data in northwestern India
754 to train and validate algorithms.

755 **5. Conclusion**

756 The two-fold problem of satellite spatial and temporal limitations poses a difficult
757 challenge for estimating burned area from agricultural fires. In particular, the small
758 landholdings in the region and the short duration of agricultural fires require both high
759 spatial and temporal satellite resolution. MODIS burned area product MCD64A1 is
760 limited by moderate spatial resolution (500 m), and the GFEDv4s small fires boost to
761 MCD64A1 further limits the spatial resolution (0.25°). In this study, we develop a
762 hybrid approach (ModL2T) that leverages the temporal resolution of MODIS (daily,
763 500 m) and spatial resolution of Landsat (every 16 days, 30 m) in a two-step NBR-
764 based classification. Additionally, we use the Google Earth Engine platform to rapidly
765 run the ModL2T algorithm using all available MODIS and Landsat images within the
766 defined pre-fire and post-fire time periods to classify post-monsoon (October to
767 November) burned area. The ModL2T algorithm estimates $66 \pm 31\%$ higher post-
768 monsoon burned area than MCD64A1 in Punjab and Haryana from 2003-2016. In
769 future work, the high-resolution BA_{ModL2T} (30 m) dataset, which moderately well agrees
770 ($r = 0.62$) with independent household survey results, can be used to build an emissions
771 inventory for post-monsoon agricultural fires in Punjab and Haryana and re-evaluate –
772 and likely previously underestimated – regional public health effects. Lastly, the
773 methods described in this study may be useful in other regions with high concentrations

774 of small fires and in improving global fire emissions inventories currently based on
775 moderate-resolution satellite products.

776 **Acknowledgements**

777 We acknowledge the Columbia University Department of Earth and Environmental
778 Sciences Young Investigator Award and Earth Institute Research Assistantship program
779 for support for this work, as well as the Columbia University President's Global
780 Innovation Fund. This work was also supported by a National Science Foundation
781 Graduate Research Fellowship awarded to T.L. (Award Number DGE1144152 and
782 DGE1745303). The household survey in 2016 was funded by a NSF SEES Postdoctoral
783 Fellowship (Award Number 1415436) to M.J. We also thank Dr Brent Holben and site
784 managers for establishing and maintaining AERONET Lahore, Pakistan site.

785 **References**

- 786 Ahmed, T., B. Ahmad, and W. Ahmad. 2015. "Why do farmers burn rice residue?
787 Examining farmers' choices in Punjab, Pakistan." *Land Use Policy* 47: 448-458.
788 doi:10.1016/j.landusepol.2015.05.004.
- 789 Avery, T. E. and G. L. Berlin. 1992. *Fundamentals of remote sensing and airphoto*
790 *interpretation*. Upper Saddle River: Prentice Hall.
- 791 Bai, R. 2014. "Analysis of the Trends of Agricultural Mechanisation Development in
792 China (2000-2020)." *ESCAP/CSAM Policy Brief*, Issue No.1. [http://www.un-](http://www.un-csam.org/publication/PB201401.pdf)
793 [csam.org/publication/PB201401.pdf](http://www.un-csam.org/publication/PB201401.pdf).
- 794 Bhullar, G. S. and N. K. Bhullar. 2013. *Agricultural Sustainability: Progress and*
795 *Prospects in Crop Research*. London: Academic Press/Elsevier.
- 796 Boschetti, L., D. P. Roy, C. O. Justice, and M. L. Humber. 2015. "MODIS–Landsat
797 fusion for large area 30 m burned area mapping." *Remote Sensing of*
798 *Environment*. 161: 27-42. doi:10.1016/j.rse.2015.01.022.
- 799 Chen, J., Ban, Y., and Li, S. "Open access to Earth land-cover map." *Nature*. 514: 434.
800 doi:10.1038/514434c.
- 801 Chen, J., Cao, X., Peng, S., and Ren, H. 2017. "Analysis and Applications of
802 GlobeLand30: A Review." *International Journal of Geo-Information*. 6: 230.
803 doi:10.3390/ijgi6080230.
- 804 Cocke, A. E., P. Z. Fulé, and J. E. Crouse. 2005. "Comparison of burn severity
805 assessments using Differenced Normalised Burn Ratio and ground data."
806 *International Journal of Wildland Fire* 14(2): 189-198. doi:10.1071/WF04010.
- 807 Cohen, J. 1960. "A coefficient of agreement for nominal scales." *Education and*
808 *Psychological Measurement* 20(1): 37-46. doi:10.1177/001316446002000104.
- 809 Cusworth, D. H., L. J. Mickley, M. P. Sulprizio, T. Liu, M. E. Marlier, R. S. DeFries, S.
810 K. Guttikunda, and P. Gupta. 2018. "Quantifying the influence of agricultural
811 fires in northwest India on urban air pollution in Delhi, India." *Environmental*
812 *Research Letters*. In Press.
- 813 Deininger, K., D. Monchuk, H. K. Nagarajan, and S. K. Singh. 2017. "Does Land
814 Fragmentation Increase the Cost of Cultivation? Evidence from India." *The*
815 *Journal of Development Studies* 53(1): 82-98. doi:
816 10.1080/00220388.2016.1166210.
- 817 Drusch, M., U. Del Bello, S. Carlier, O. Colin, V. Fernandez, F. Gascon, B. Hoersch, C.
818 Isola, P. Laberinti, P. Martimort, A. Meygret, F. Spoto, O. Sy, F. Marchese, and
819 P. Bargellini. 2012. "Sentinel-2: ESA's optical high-resolution mission for
820 GMES operational services." *Remote Sensing of Environment* 120: 25–36. doi:
821 10.1016/j.rse.2011.11.026
- 822 Eva, H. and E. F. Lambin. 1998. "Burnt area mapping in Central Africa using ATSR
823 data." *International Journal of Remote Sensing* 19(18): 3473-3497.
824 doi:10.1080/014311698213768.
- 825 Giglio, L. 2007. "Characterisation of the tropical diurnal fire cycle using VIRS and
826 MODIS observations." *Remote Sensing of Environment* 108(4): 407-421.
827 doi:10.1016/j.rse.2006.11.018.

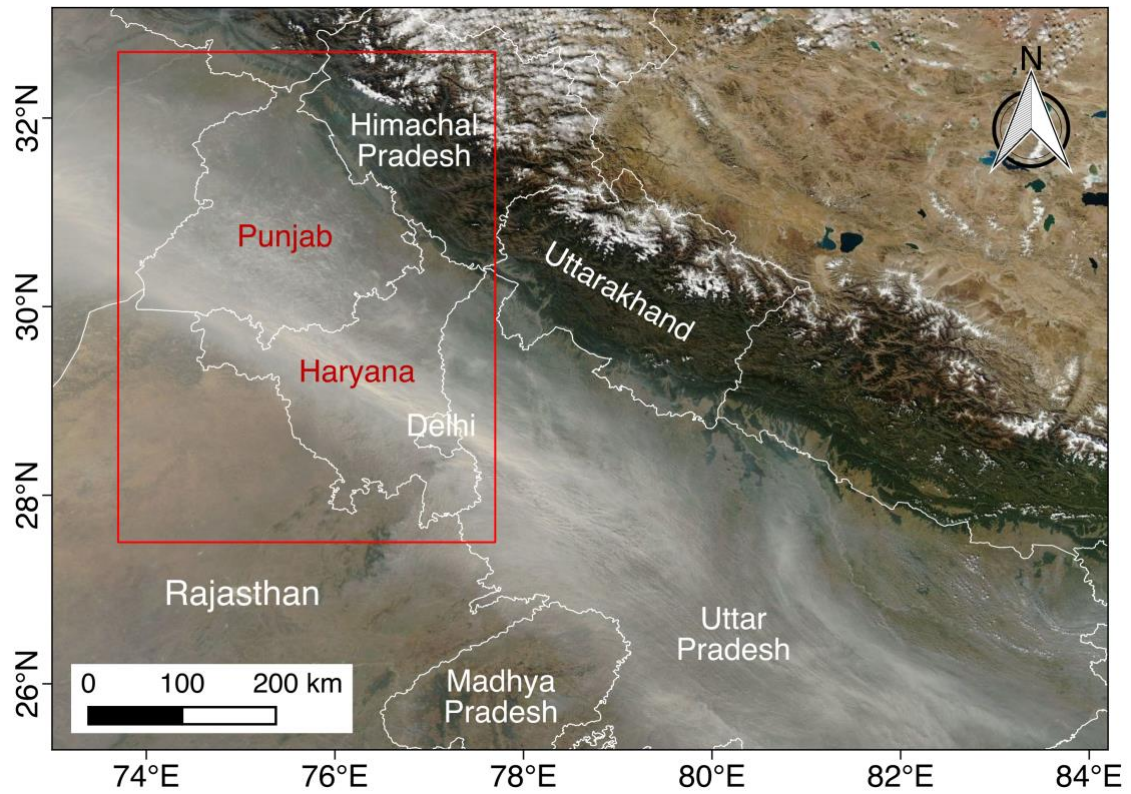
- 828 Giglio, L., T. Loboda, D. P. Roy, B. Quayle, and C. O. Justice. 2009. “An active-fire
829 based burned area mapping algorithm for the MODIS sensor.” *Remote Sensing*
830 *of Environment* 113(2): 408-420. doi:10.1016/j.rse.2008.10.006.
- 831 Giglio, L., J. T. Randerson, and G. R. van der Werf. 2013. “Analysis of daily, monthly,
832 and annual burned area of the fourth-generation global fire emissions database
833 (GFED4).” *Journal of Geophysical Research* 118(1): 317-328.
834 doi:10.1002/jgrg.20042.
- 835 Giglio, L. 2015. “MODIS Collection 6 Active Fire Product User’s Guide Revision A.”
836 https://cdn.earthdata.nasa.gov/conduit/upload/3865/MODIS_C6_Fire_User_Guide_A.pdf
837
- 838 Giglio, L., L. Boschetti, D. Roy, A. A. Hoffmann, and M. Humber. 2016. “Collection 6
839 MODIS Burned Area Product User’s Guide Version 1.0.” [http://modis-](http://modis-fire.umd.edu/files/MODIS_C6_BA_User_Guide_1.0.pdf)
840 [fire.umd.edu/files/MODIS_C6_BA_User_Guide_1.0.pdf](http://modis-fire.umd.edu/files/MODIS_C6_BA_User_Guide_1.0.pdf)
- 841 Gorelick, N., M. Hancher, M. Dixon, S. Ilyushchenko, D. Thau, and R. Moore. 2017.
842 “Google Earth Engine: Planetary-scale geospatial analysis for
843 everyone.” *Remote Sensing of Environment*. 202: 18-27.
844 doi:10.1016/j.rse.2017.06.031.
- 845 Government of Punjab. 2007. *State of environment*. Chandigarh: Punjab State Council
846 of Science and Technology.
- 847 Gupta, R. 2012. *Causes of Emissions from Agricultural Residue Burning in North-West*
848 *India: Evaluation of a Technology Policy Response*. SANDEE Working Paper
849 No. 66–12.
- 850 Hall, J. V., T. V. Loboda, L. Giglio, and G. W. McCarty. 2016. “A MODIS-based
851 burned area assessment for Russian croplands: Mapping requirements and
852 challenges.” *Remote Sensing of Environment*. 184: 506-521.
- 853 Jain, N., A. Bhatia, and H. Pathak. 2014. “Emission of Air Pollutants from Crop
854 Residue Burning in India.” *Aerosol and Air Quality Research*. 14: 422-430.
855 doi:10.4209/aaqr.2013.01.0031.
- 856 Kaskaoutis, D. G., S. Kumar, D. Sharma, R. P. Singh, S. K. Kharol, M. Sharma, A. K.
857 Singh, S. Singh, A. Singh, and D. Singh. 2014. “Effects of crop residue burning
858 on aerosol properties, plume characteristics, and long-range transport over
859 northern India.” *Journal of Geophysical Research*. 119: 5424–5444, doi:
860 10.1002/2013JD021357.
- 861 Key, C. H. and N. C. Benson. 2006. “Landscape assessment (LA): Sampling and
862 analysis methods. In D. C. Lutes, R. E. Keane, J. F. Caratti, C. H. Key, N. C.
863 Benson, S. Sutherland, and L. J. Gangi (Eds.)” *FIREMON: Fire effects*
864 *monitoring and inventory system*. General Technical Report RMRS-GTR-164-
865 CD (pp. LA1–LA51). Rocky Mountain Research Station, Fort Collins, CO:
866 United States Department of Agriculture, Forest Service.
867 http://www.fs.fed.us/rm/pubs/rmrs_gtr164.pdf.
- 868 Kumar, P., S. Kumar, and L. Joshi. 2015. *Socioeconomic and Environmental*
869 *Implications of Agricultural Residue Burning: A Case Study of Punjab, India*.
- 870 Landis, J. R. and G. G. Kock. 1977. “The Measurement of Observer Agreement for
871 Categorical Data.” *Biometrics* 33(1): 159-174. doi:10.2307/2529310.
- 872 Levy, R. C., S. Mattoo, L. A. Munchak, L. A. Remer, A. M. Sayer, F. Patadia, and N.

- 873 C. Hsu. 2013. "The Collection 6 MODIS aerosol products over land and ocean."
874 *Atmospheric Measurement Techniques* 6(11): 2989-3034. doi:10.5194/amt-6-
875 2989-2013.
- 876 Lewis, S. A., A. T. Hudak, R. D. Ottmar, P. R. Robichaud, L. B. Lentile, S. M. Hood, J.
877 B. Cronan, and P. Morgan. 2011. Using hyperspectral imagery to estimate forest
878 floor consumption from wildfire in boreal forests of Alaska, USA. *International*
879 *Journal of Wildland Fire*. 20: 255-271. doi:10.1071/WF09081.
- 880 Liu, T., M. E. Marlier, R. S. DeFries, D. M. Westervelt, K. R. Xia, A. M. Fiore, L. J.
881 Mickley, D. H. Cusworth, and G. Milly. 2018. "Seasonal impact of regional
882 outdoor biomass burning on air pollution in three Indian cities: Delhi,
883 Bengaluru, and Pune." *Atmospheric Environment*. 172: 83-92.
884 doi:10.1016/j.atmosenv.2017.10.024.
- 885 Loboda, T., K. J. O'Neal, and I. Csiszar. 2007. "Regionally adaptable dNBR-based
886 algorithm for burned area mapping from MODIS data." *Remote Sensing of*
887 *Environment* 109(4): 429-442. doi:10.1016/j.rse.2007.01.017.
- 888 Mahajan, G., V. Kumar, and B. S. Chauhan. 2017. "Rice Production in India." In: B.
889 Chauhan, K. Jabran, G. Mahajan G. (eds). *Rice Production Worldwide*.
890 Springer, Cham. doi:10.1007/978-3-319-47516-5_3.
- 891 McCarty, J. L., S. Korontzi, and S. Trigg. 2008. "A hybrid remote sensing approach to
892 quantifying crop residue burning in the United States." *Applied Engineering in*
893 *Agriculture* 24(4): 515-527. doi:10.13031/2013.25137.
- 894 McCarty, J. L., S. Korontzi, C. O. Justice, and T. Loboda. 2009. "The spatial and
895 temporal distribution of crop residue burning in the contiguous United States."
896 *Science of The Total Environment* 407(15): 5701-5712.
897 doi:10.1016/j.scitotenv.2009.07.009.
- 898 Mehta, C. R., N. S. Chandel, T. Senthilkumar, and K. K. Singh. 2014. "Trends of
899 Agricultural Mechanisation in India." *ESCAP/CSAM Policy Brief*, Issue No. 2.
900 <http://www.un-csam.org/publication/PB201402.pdf>.
- 901 Misri, B. K. 1999. *Country Pasture/Forage Resources Profiles, India*.
902 <http://www.fao.org/ag/AGP/AGPC/doc/Counprof/India.htm>.
- 903 Mu, M., J. T. Randerson, G. R. van der Werf, L. Giglio, P. Kasibhatla, D. Morton, G.
904 J. Collatz, R. S. DeFries, E. J. Hyer, E. M. Prins, D. W. T. Griffith, D.
905 Wunch, G. C. Toon, V. Sherlock, and P. O. Wennberg. 2011. "Daily and 3-
906 hourly variability in global fire emissions and consequences for atmospheric
907 model predictions of carbon monoxide." *Journal of Geophysical Research:*
908 *Atmospheres*. 116: D24303. doi:10.1029/2011JD016245.
- 909 Munchak, L. A., R. C. Levy, S. Mattoo, L. A. Remer, B. N. Holben, J. S. Schafer, C. A.
910 Hostetler, and R. A. Ferrare. 2013. "MODIS 3 km aerosol product: applications
911 over land in an urban/suburban region." *Atmospheric Measurement Techniques*
912 6(7): 1747-1759. doi:10.5194/amt-6-1747-2013.
- 913 Oliva, P. and W. Schroeder. 2015. "Assessment of VIIRS 375 m active fire detection
914 product for direct burned area mapping." *Remote Sensing of Environment* 160:
915 144-155. doi:10.1016/j.rse.2015.01.010.
- 916 Picotte, J. J. and K. M. Robertson. 2010. "Accuracy of remote sensing wildland fire-
917 burned area in southeastern U.S. Coastal Plain habitats." In K. M. Robertson, K.

- 918 E. M. Galley, and R. E. Masters (eds.). *Proceedings of the 24th Tall Timbers*
 919 *Fire Ecology Conference: The Future of Prescribed Fire: Public Awareness,*
 920 *Health, and Safety. Tall Timbers Research Station, Tallahassee, Florida, USA.*
- 921 Pleniou, M. and N. Koutsias. 2013. "Sensitivity of spectral reflectance values to
 922 different burn and vegetation ratios: A multi-scale approach applied in a fire
 923 affected area." *ISPRS Journal of Photogrammetry and Remote Sensing* 79: 199-
 924 210. doi:10.1016/j.isprsjprs.2013.02.016.
- 925 Punia, M., V. P. Nautiyal, and Y. Kant. 2008. "Identifying biomass burned patches of
 926 agriculture residue using satellite remote sensing data." *Current Science* 94(9):
 927 1185-1190.
- 928 Punjab Remote Sensing Centre (PRSC), Ludhiana. 2015. *Monitoring Residue Burning*
 929 *through Satellite Remote Sensing.* Punjab Pollution Control Board, Patiala.
- 930 Randerson, J. T., Y. Chen, G. R. van der Werf, B. M. Rodgers, and D. C. Morton. 2012.
 931 "Global burned area and biomass burning emissions from small fires." *Journal*
 932 *of Geophysical Research* 117(4): G04012. doi:10.1029/2012JG002128.
- 933 Rogan, J. and S. R. Yool. 2001. "Mapping fire-induced vegetation depletion in the
 934 Peloncillo Mountains: Arizona and New Mexico." *International Journal of*
 935 *Remote Sensing* 22(16): 3101-3121. doi:10.1080/01431160152558279.
- 936 Roy, D. P. 1999. "Multi-temporal active-fire based burn scar detection algorithm."
 937 *International Journal of Remote Sensing* 20(5): 1031-1038.
 938 doi:10.1080/014311699213073.
- 939 Roy, D. P., Y. Jin, P. E. Lewis, and C. O. Justice. 2005. "Prototyping a global algorithm
 940 for systematic fire-affected area mapping using MODIS time series data."
 941 *Remote Sensing of Environment* 97(2): 137-162. doi:10.1016/j.rse.2005.04.007.
- 942 Sayer, A. M., N. C. Hsu, C. Bettenhausen, and M-J. Jeong. 2013. "Validation and
 943 uncertainty estimates for MODIS Collection 6 "Deep Blue" aerosol data."
 944 *Journal of Geophysical Research: Atmospheres* 118(14): 7864-7872.
 945 doi:10.1002/jgrd.50600.
- 946 Sharma, A. R., S. K. Kharol, K. V. S. Badarinath, and D. Singh. 2010. "Impact of
 947 agriculture crop residue burning on atmospheric aerosol loading – a study over
 948 Punjab State, India." *Annales Geophysicae* 28(2): 367-379.
- 949 Sidhu, B. S., and V. Beri. 2005. "Experience with managing rice residues in intensive
 950 rice-wheat cropping system in Punjab." In I. P. Abrol, R. K. Gupta, and R. K.
 951 Malik (Eds.), *Conservation agriculture: Status and prospects* 55-63. New Delhi:
 952 Centre for Advancement of Sustainable Agriculture, National Agriculture
 953 Science Centre.
- 954 Singh, G., Y. Kant, and V. K. Dadhwal. 2009. "Remote sensing of crop residue burning
 955 in Punjab (India): a study on burned area estimation using multi-sensor
 956 approach." *Geocarto International* 24(4): 273-292.
 957 doi:10.1080/10106040802556181.
- 958 Singh, K. 2009. "Act to Save Groundwater in Punjab: Its Impact on Water Table,
 959 Electricity Subsidy and Environment." *Agricultural Economics Research*
 960 *Review* 22: 365-386.
- 961 Singh, M. K., R. Gautam, and P. Venkatachalam 2017. "Bayesian Merging of MISR
 962 and MODIS Aerosol Optical Depth Products Using Error Distributions From

- 963 AERONET.” *IEEE Journal of Selected Topics in Applied Earth Observations*
964 *and Remote Sensing* PP(99): 1-15. doi:10.1109/JSTARS.2017.2734331.
- 965 Singh, R. P., H. S. Dhaliwal, H. S. Sidhu, Y. S. Manpreet-Singh, and J. Blackwell.
966 2008. “Economic assessment of the Happy Seeder for rice-wheat systems in
967 Punjab, India.” Conference Paper, AARES 52nd Annual conference, Canberra.
968 Australia: ACT.
- 969 Strauss, M. 2017. “Planet Earth to get a daily selfie.” *Science* 355(6327): 782-783.
970 doi:10.1126/science.355.6327.782.
- 971 Thumaty, K. C., S. R. Rodda, J. Singhal, R. Gopalakrishnan, C. S. Jha, G. D. Parsi, and
972 V. K. Dadhwal. 2015. “Spatio-temporal characterisation of agriculture residue
973 burning in Punjab and Haryana, India, using MODIS and Suomi NPP VIIRS
974 data.” *Current Science* 109(10): 1850-1855. doi:10.18520/v109/i10/1850-1855.
- 975 Vadrevu, K. P., E. Ellicott, and K. Badarinath. 2011. “MODIS derived fire
976 characteristics and aerosol optical depth variations during the agricultural
977 residue burning season, north India.” *Environmental Pollution* 159(6): 1560-
978 1569. doi:10.1016/j.envpol.2011.03.001.
- 979 van der Werf, G. R., J. T. Randerson, L. Giglio, G. J. Collatz, M. Mu, P. S. Kasibhatia,
980 D. C. Morton, R. S. DeFries, Y. Jin, and T. T. van Leeuwen. 2010. “Global fire
981 emissions and the contribution of deforestation, savanna, forest, agricultural, and
982 peat fires (1997-2009).” *Atmospheric Chemistry and Physics* 10(23): 11707-
983 11735. doi:10.5194/acp-10-11707-2010.
- 984 van der Werf, G. R., J. T. Randerson, L. Giglio, T. T. van Leeuwen, Y. Chen, B. M.
985 Rogers, M. Mu, M. J. E. van Marle, D. C. Morton, G. J. Collatz, R. J. Yokelson,
986 P. S. Kasibhatla. 2017. “Global fire estimates during 1997-2016.” *Earth System*
987 *Science Data* 9:687-720. doi:10.5194/essd-2016-62.
- 988 Veraverbeke, S., W. W. Verstraeten, S. Lhermitte, and R. Goossens. 2010.
989 “Illumination effects on the differenced Normalized Burn Ratio’s optimality for
990 assessing fire severity.” *International Journal of Applied Earth Observation and*
991 *Geoinformation*. 12: 60-70. doi:10.1016/J.JAG.2009.10.004.
- 992 Vermote, E. F. and S. Kotchenova. 2008. “Atmospheric correction for the monitoring of
993 land surfaces.” *Journal of Geophys Research* 113: D23S90.
994 doi:10.1029/2007JD009662
- 995 United Nations, Department of Economic and Social Affairs, Population Division.
996 2015. *World Population Prospects: The 2015 Revision, Key Findings and*
997 *Advance Tables Working Paper No. ESA/P/WP.241.*
- 998 Wang, Q., G. A. Blackburn, A. O. Onojeghuo, J. Dash, L. Zhou, Y. Zhang, and P. M.
999 Atkinson. 2017. “Fusion of Landsat 8 OLI and Sentinel-2 MSI Data.” *IEEE*
1000 *Transactions on Geoscience and Remote Sensing* 55(7): 3885-3899. doi:
1001 10.1109/TGRS.2017.2683444.
- 1002 Wang, S., M. H. A. Baig, S. Liu, H. Wan, T. Wu, and Y. Yang. 2018. “Estimating the
1003 area burned by agricultural fires from Landsat 8 Data using the Vegetation
1004 Difference Index and Burn Scar Index.” *International Journal of Wildland Fire*.
1005 27(4): 217-227. doi: 10.1071/WF17069.
- 1006 Xiang, H.-B. 2013. “Algorithms for Moderate Resolution Imaging Spectroradiometer
1007 cloud-free image compositing.” *Journal of Applied Remote Sensing* 7: 073486.

- 1008 doi: 10.1117/1.JRS.7.073486.
- 1009 Yadav, M., M. P. Sharma, R. Prawasi, R. Khichi, P. Kumar, V. P. Mandal, A. Salim,
1010 and R. S. Hooda. 2014a. "Estimation of Wheat/Rice Residue Burning Areas in
1011 Major Districts of Haryana, India, Using Remote Sensing Data." *Journal of the*
1012 *Indian Society of Remote Sensing*. 42(2): 343-352. doi:10.1007/s12524-013-
1013 0330-z.
- 1014 Yadav, M., R. Prawasi, S. Jangra, P. Rana, K. Kumari, S. Lal, K. Jakhar, S. Sharma, and
1015 R. S. Hooda. 2014b. "Monitoring seasonal progress of rice stubble burning in
1016 districts of Haryana, India, using multirate AwiFS data." *The International*
1017 *Archives of the Photogrammetry, Remote Sensing and Spatial Information*
1018 *Sciences*. 40(8): 1003-1009. doi:10.5194/isprsarchives-XL-8-1003-2014.
- 1019 Zhu, C., H. Kobayashi, Y. Kanaya, and M. Saito. 2017. Size-dependent validation of
1020 MODIS MCD64A1 burned area over six vegetation types in boreal Eurasia:
1021 Large underestimation in croplands. *Scientific Reports*. 7: 4181.
1022 doi:10.1038/s41598-017-03739-0.



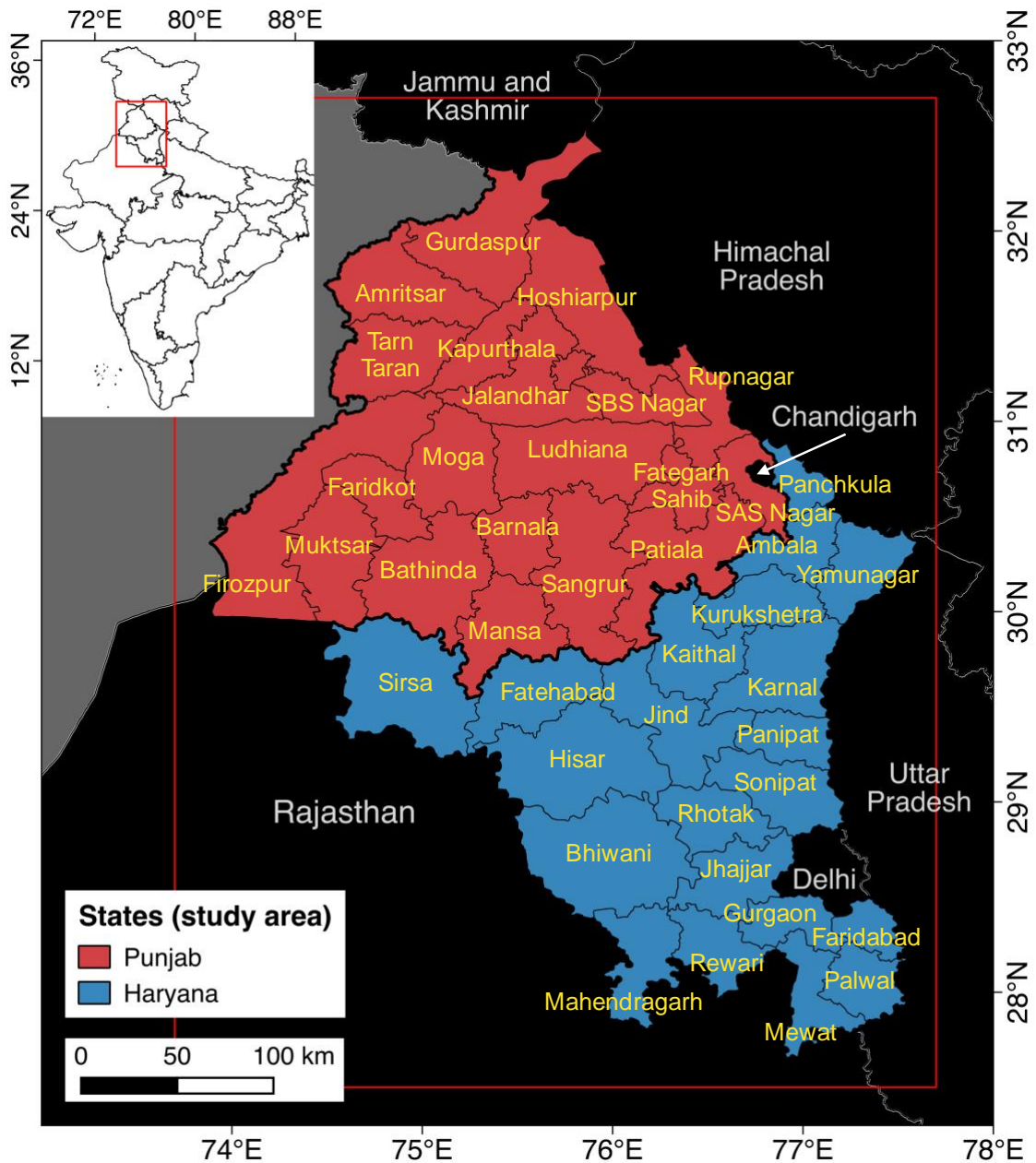
1023

1024

1025

1026

Figure 1. Example of thick haze over northern India during the post-monsoon burning season: True colour MODIS/Aqua on November 6, 2016 (NASA Worldview). The study area is bounded by a red box.



1027

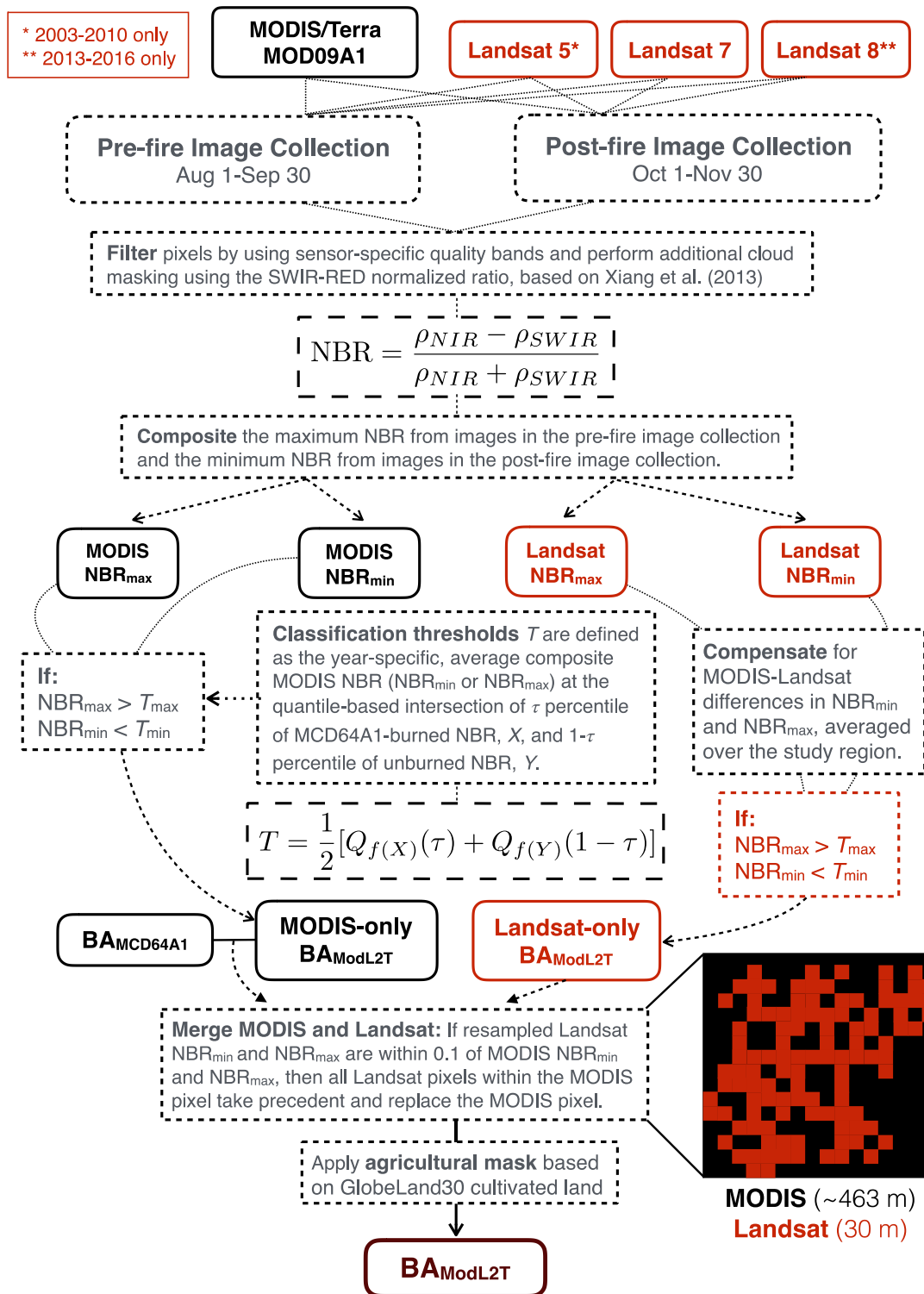
1028

1029

1030

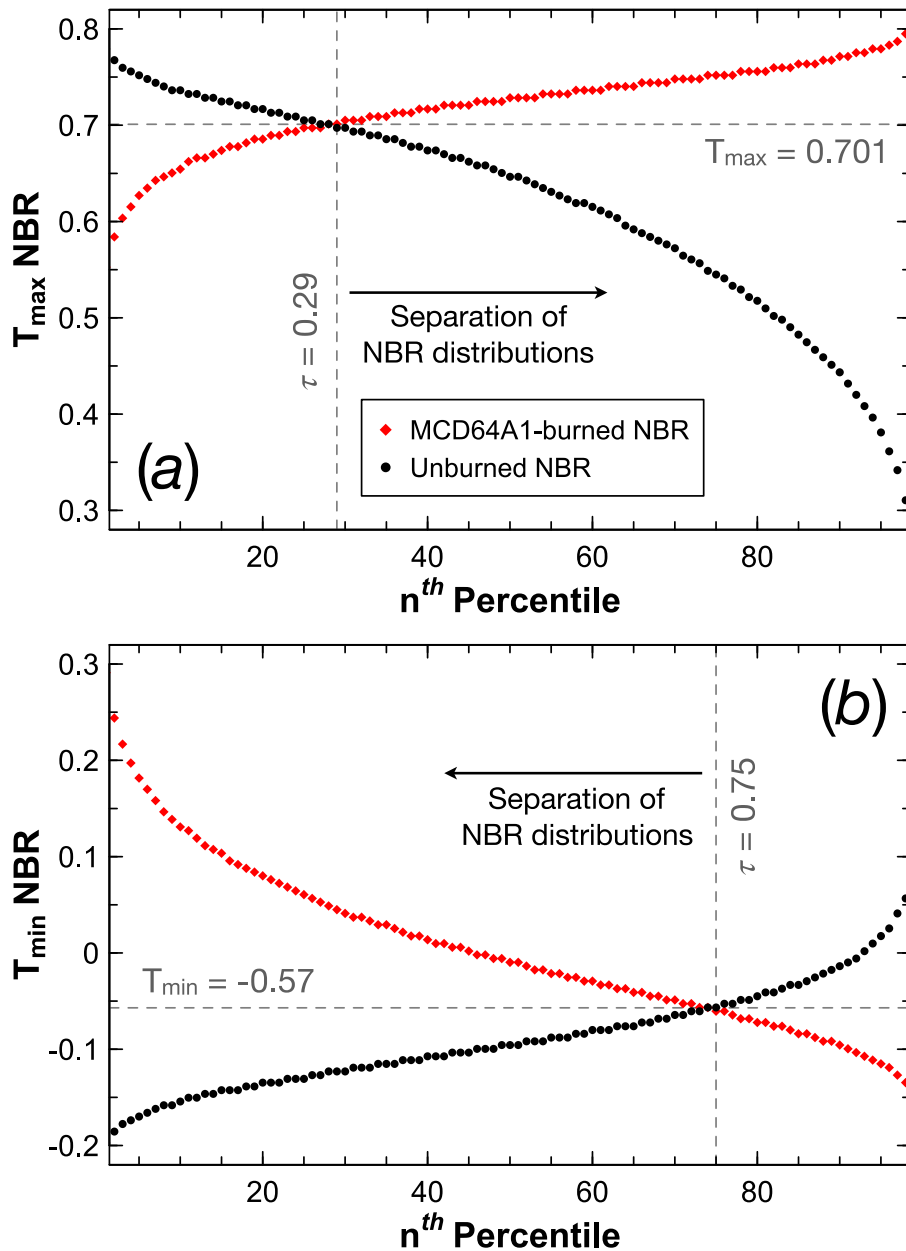
1031

Figure 2. District-level maps of the study area: Punjab (red) and Haryana (blue), two agricultural states in northwestern India. District administrative borders are from the 2011 Indian census. *Inset:* The red box shows the location of the study area in a zoomed-out view of states in India, excluding the seven sister states.



1032

1033 **Figure 3. Workflow of the ModL2T algorithm:** estimation of post-monsoon
 1034 (October-November) agricultural burned area. The final ModL2T burned area is 30 m x
 1035 30 m in spatial resolution. The inset schematic shows Landsat burned pixels (red)
 1036 overlain on a MODIS burned pixel (black); if the MODIS-Landsat merging criteria are
 1037 met, then the ~238 Landsat pixels replace the MODIS pixel.



1038

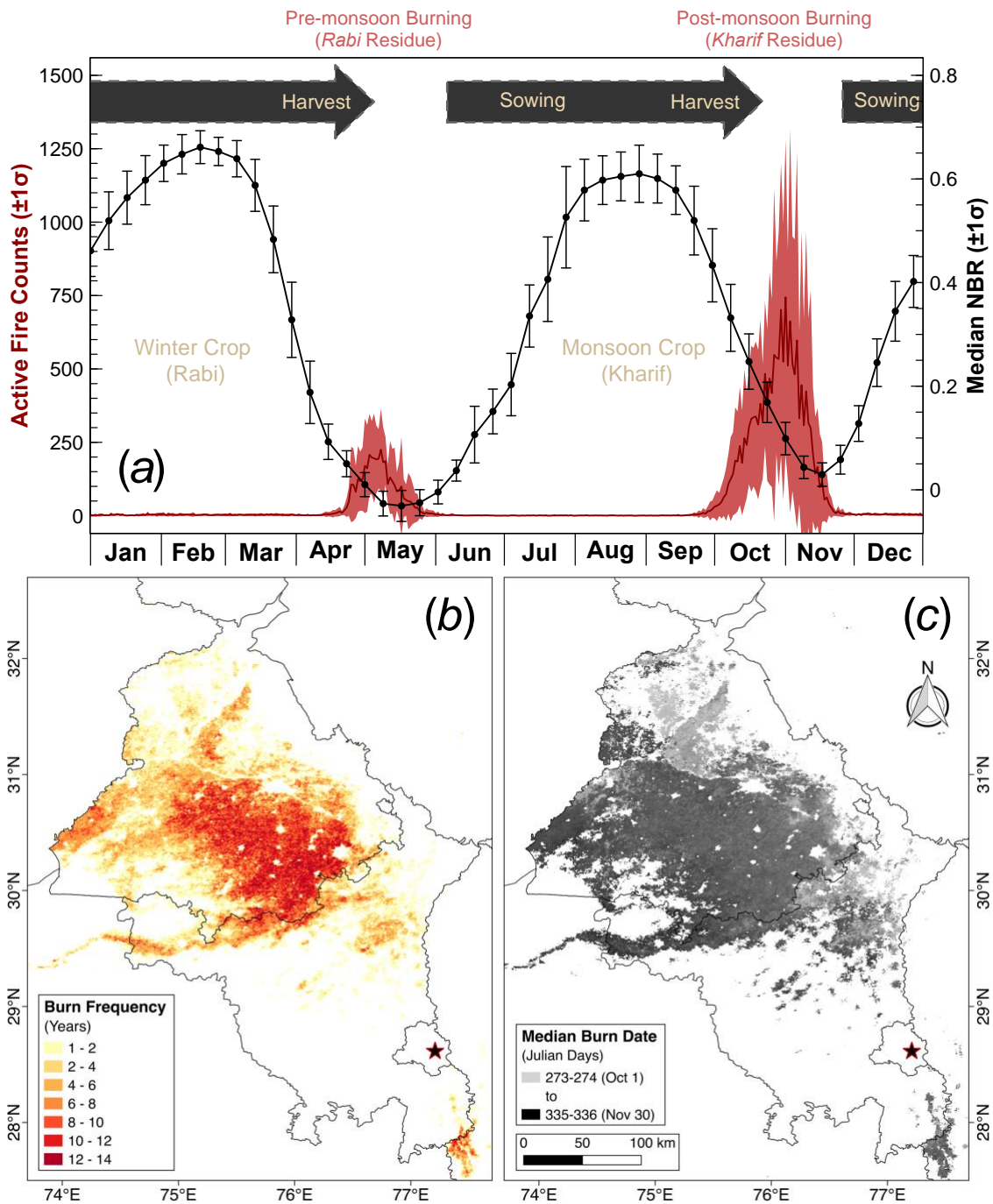
1039

1040

1041

1042

Figure 4. Example of thresholds T_{min} and T_{max} derived for post-monsoon 2016: thresholds T_{min} and T_{max} for the ModL2T algorithm (Figure 3) are derived from the τ percentile separation of MCD64A1-burned NBR and unburned NBR distributions in agricultural areas.



1043

1044

1045

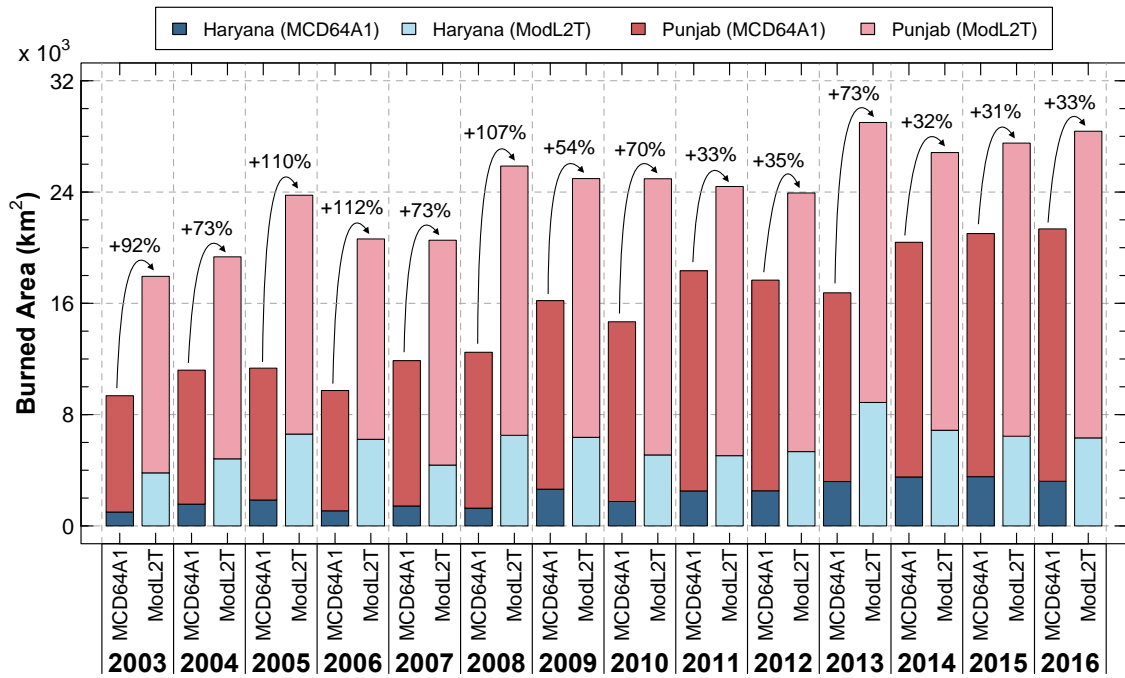
1046

1047

1048

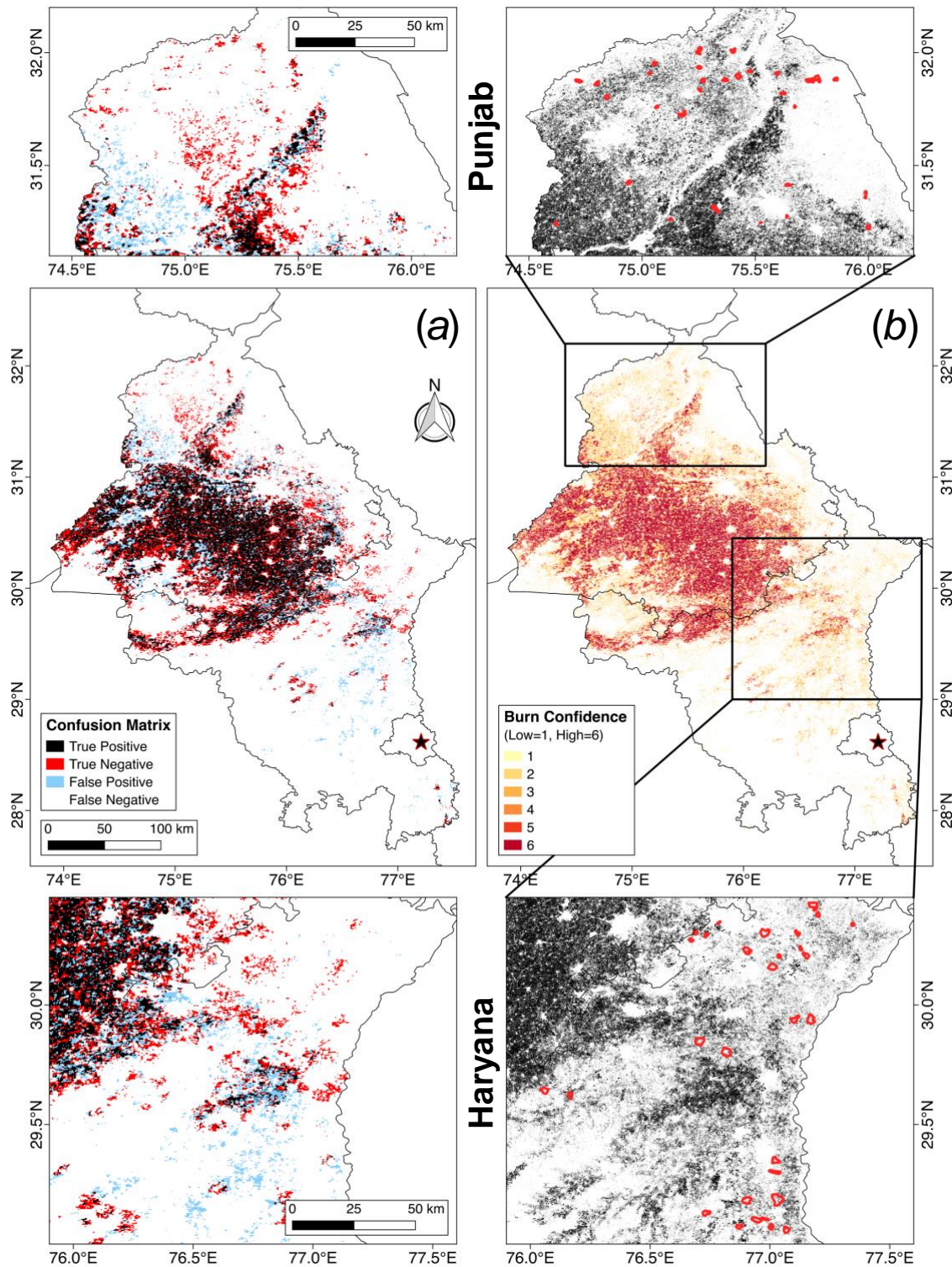
1049

Figure 5. Spatio-temporal overview of agricultural burning in northwestern India:
 (a) The double crop-fire cycle, following Vadrevu et al. (2011), using daily MODIS fire counts and 8-day composite median NBR, with $\pm 1\sigma$ envelopes, in Punjab and Haryana, 2003-2016. Post-monsoon (October-November) (b) burn frequency and (c) median burn date based on BAmCD64A1. The colour bar is discrete in (b) and continuous in (c). The star denotes the location of New Delhi.



1050

1051 **Figure 6. Total agricultural burned area: $BA_{MCD64A1}$ and BA_{ModL2T} in Punjab (red**
 1052 **shades) and Haryana (blue shades) during post-monsoon (October-November), 2003-**
 1053 **2016. The ModL2T algorithm estimates $66 \pm 31\%$ higher post-monsoon burned area in**
 1054 **Punjab and Haryana than MCD64A1. The curved arrows denote the relative increase in**
 1055 **burned area mapped by ModL2T compared to MCD64A1.**



1056

1057

1058

1059

1060

1061

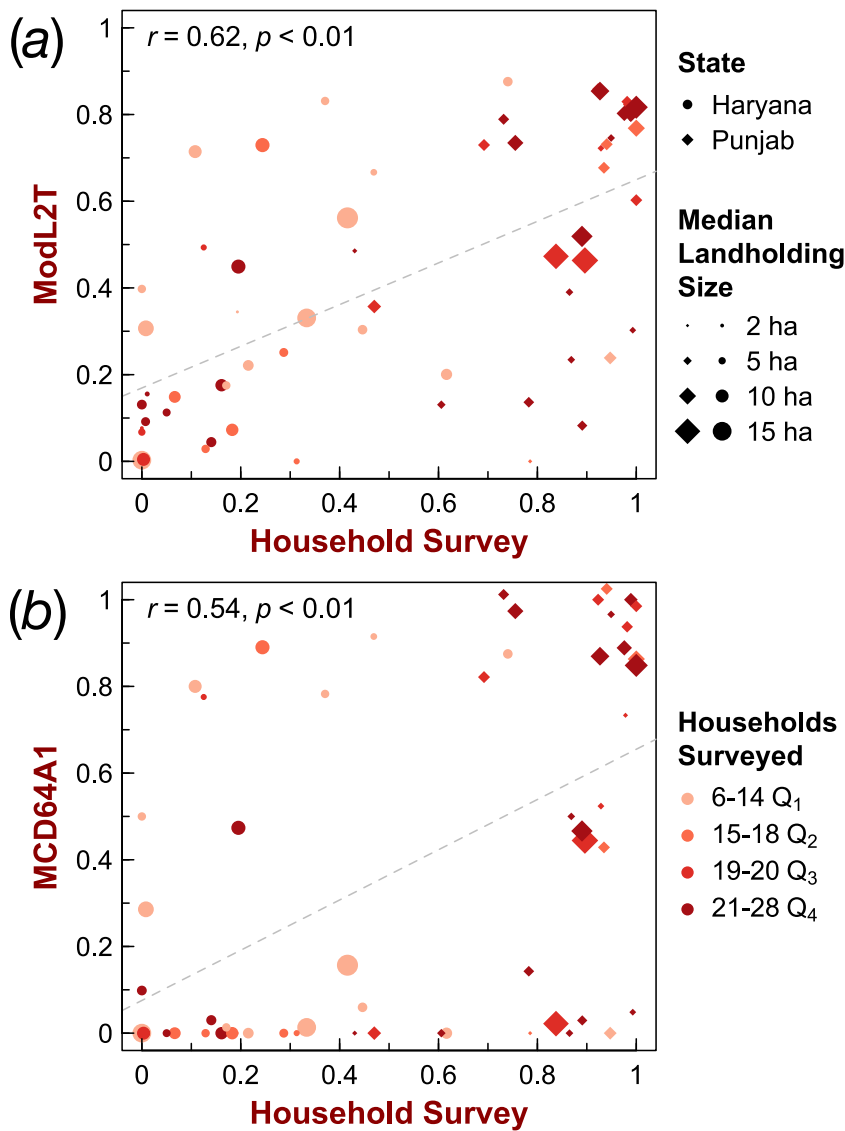
1062

Figure 7. ModL2T burned area classification: (a) Agreement between $BA_{MCD64A1}$ and MODIS-only BA_{ModL2T} and (b) classification confidence (Low = 1, High = 6) for BA_{ModL2T} in Haryana and Punjab, post-monsoon (October-November) in 2016. The zoomed-in images show BA_{ModL2T} (black) and the locations of the villages (red polygons) in Punjab (top row) and Haryana (bottom row) surveyed in 2016 for validation. The star denotes the location of New Delhi.

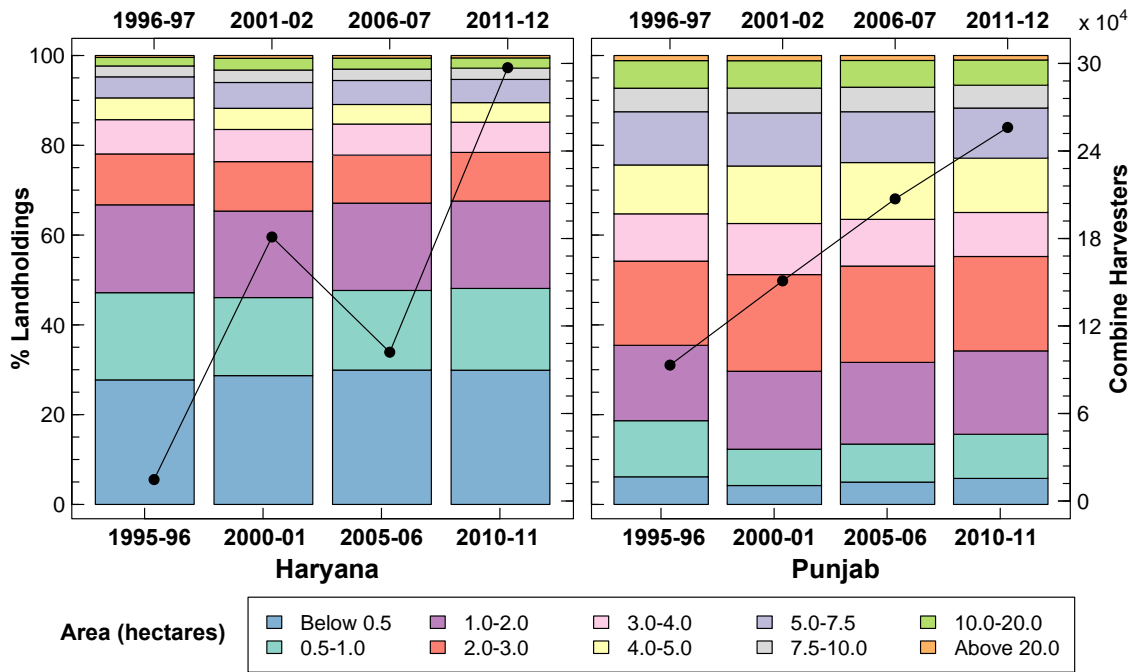
1063 **Table 1.** Geographical accuracy assessment of $BA_{MCD64A1}$ (reference) and MODIS-only
 1064 BA_{ModL2T} , in Punjab and Haryana, post-monsoon (October-November) in 2016 ($\kappa =$
 1065 0.53, moderate agreement)

MODIS-only BA_{ModL2T}	MCD64A1		Producer's Accuracy
	Burned	Unburned	
Burned	67634	49511	0.58
Unburned	31482	362183	0.92
User's Accuracy	0.68	0.88	0.84

1067

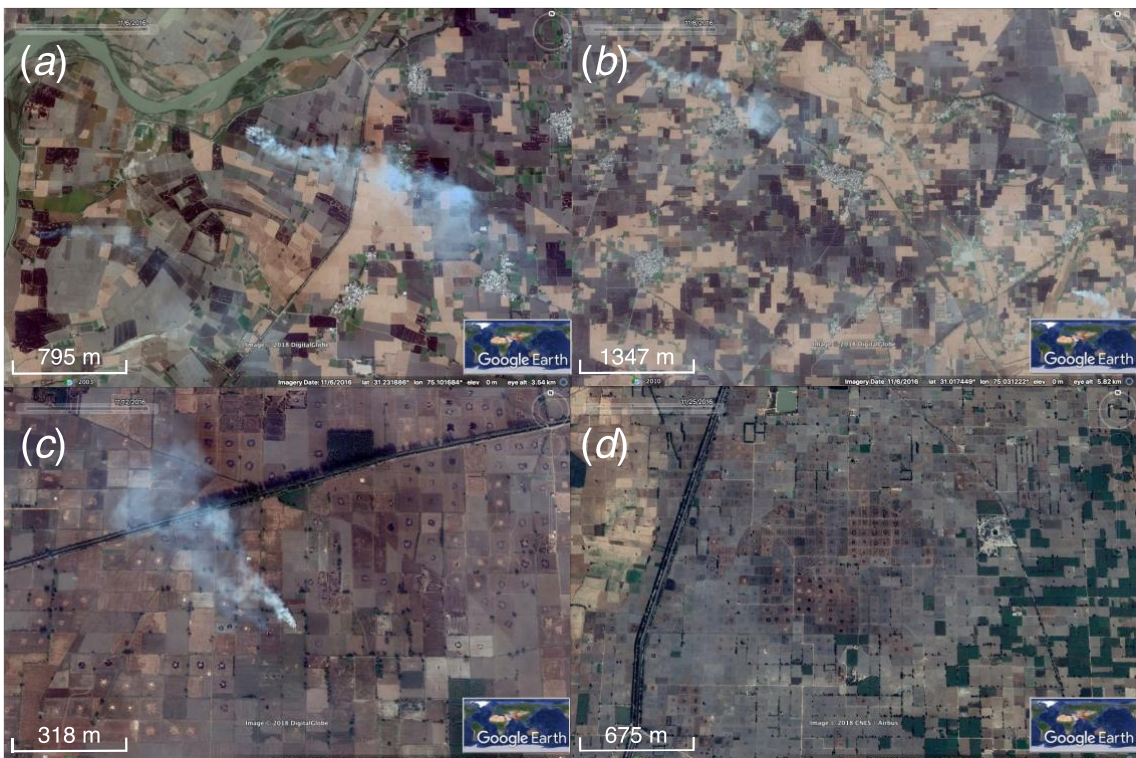


1068 **Figure 8. Validation of satellite-derived burned area using household surveys:**
 1069 comparison of % burning activity, normalised by landholding size, and % burned area
 1070 from (a) ModL2T and (b) MCD64A1 in 30 Punjab (diamonds) and 32 Haryana (circles)
 1071 villages during post-monsoon (October-November) in 2016. The size of the markers
 1072 denotes the median landholding size, and the colour denotes the quartile of the number
 1073 of households surveyed.
 1074



1075
 1076
 1077
 1078
 1079
 1080

Figure 9. Trends in landholdings by size and in use of combine harvesters in Punjab and Haryana: Data from the Agricultural Census are in quinquennial intervals from 1995-96 to 2010-11 (landholdings) and the Input Survey, from 1996-97 to 2011-12 (combine harvesters).



1081
 1082
 1083
 1084
 1085

Figure 10. Two crop residue burning practices: Fine-resolution Google Earth DigitalGlobe and CNES/Airbus historical imagery of smoke and burn scars from crop residue burning in (a-b) central-northern Punjab (whole field) and (c-d) central Haryana (primarily partial field) in November 2016.